Lattice QCD calculation of $K \to \ell\nu_\ell\ell'^+\ell'^-$ decay width

Xin-Yu Tuo,[1] Xu Feng,[1,2,3,*] Lu-Chang Jin,[4,5] and Teng Wang[1]

[1]*School of Physics and State Key Laboratory of Nuclear Physics and Technology, Peking University, Beijing 100871, China*

[2]*Collaborative Innovation Center of Quantum Matter, Beijing 100871, China*

[3]*Center for High Energy Physics, Peking University, Beijing 100871, China*

[4]*Department of Physics, University of Connecticut, Storrs, Connecticut 06269, USA*

[5]*RIKEN-BNL Research Center, Brookhaven National Laboratory, Building 510, Upton, New York 11973, USA*

(Received 23 March 2021; accepted 1 March 2022; published 28 March 2022)

We develop a methodology for the computation of the $K \to \ell\nu_\ell\ell'^+\ell'^-$ decay width using lattice QCD and present an exploratory study here. We use a scalar function method to account for the momentum dependence of the decay amplitude and adopt the infinite-volume reconstruction method to reduce the systematic errors such as the temporal truncation effects and the finite-volume effects. We then perform a four-body phase-space integral to obtain the decay width. The only remaining technical problem is the possible power-law finite-volume effects associated with the process of $K \to \pi\pi\ell\nu_\ell \to \ell\nu_\ell\ell'^+\ell'^-$, where the intermediate state involves multiple hadrons. In this work, we use a gauge ensemble of a twisted-mass fermion with a pion mass $m_\pi = 352$ MeV and a nearly physical kaon mass. At this kinematics, the $\pi\pi$ in the intermediate state cannot be on shell simultaneously, as $2m_\pi > m_K$, and the finite-volume effects associated with the $\pi\pi$ state are exponentially suppressed. Using the developed methods mentioned above, we calculate the branching ratios for four channels of $K \to \ell\nu_\ell\ell'^+\ell'^-$, and obtain the results comparable to the experimental measurements and ChPT predictions. Our work demonstrates the capability of lattice QCD to improve the Standard Model prediction in the $K \to \ell\nu_\ell\ell'^+\ell'^-$ decay width.

DOI: 10.1103/PhysRevD.105.054518

I. INTRODUCTION

Kaon decays, especially some rare kaon decays with ultrasmall branching ratios, play an important role in current high-precision tests of the Standard Model, and they provide excellent channels to probe physics beyond the Standard Model [1]. The experimental and theoretical studies of kaon decays are believed to be more and more important nowadays, because kaon decays have both theoretically clean branching ratios in experimental searches and gradually improved Standard Model predictions [2].

As a typical rare decay, $K \to \ell\nu_\ell\ell'^+\ell'^-$ involves the second-order electroweak interaction, providing a good place to test Standard Model predictions. In experiments, three types of $K \to \ell\nu_\ell\ell'^+\ell'^-$ decays have been observed: $K \to e\nu_e e^+e^-$, $K \to \mu\nu_\mu e^+e^-$, and $K \to e\nu_e\mu^+\mu^-$, with small branching ratios on the order of $O(10^{-8})$ [3,4].

In theoretical study, the determination of the $K \to \ell\nu_\ell\ell'^+\ell'^-$ decay width is highly nontrivial due to the nonperturbative nature of kaon internal structure. Since the phase space of $K \to \ell\nu_\ell\ell'^+\ell'^-$ allows the virtual photon to carry relatively large momentum—e.g., the momentum close to the kaon mass—understanding the momentum dependence of the decay amplitude is essential in the theoretical calculation of the $K \to \ell\nu_\ell\ell'^+\ell'^-$ decay width. To be specific, apart from the decay constant which describes the pointlike interaction, four form factors are involved to describe the structure-dependent contribution in $K \to \ell\nu_\ell\ell'^+\ell'^-$ [5]. The momentum dependence of these form factors is non-negligible. In experiments, it produces different results by treating the form factors as constants or considering the relevant momentum dependence through a simple vector-meson-dominance model [3]. Therefore, properly including the momentum dependence of the decay amplitude is important for both theoretical predictions and experimental measurements.

Theoretical study of the $K \to \ell\nu_\ell\ell'^+\ell'^-$ amplitude and form factors has been carried out using chiral perturbation theory (ChPT) [5], where form factors are estimated at the next-to-leading order (NLO), and predictions close to experimental results are obtained. However, one should

*xu.feng@pku.edu.cn

note that the form factors F_V and F_A are treated as constants at NLO [5], and the momentum dependence only appears at next-to-next-to-leading order (NNLO) [6,7]. Thus, the theoretical uncertainties due to momentum dependence have not been estimated thoroughly by the past ChPT studies, which leads to a difficulty to directly compare the results between experiments and ChPT.

As a generic nonperturbative approach, lattice QCD can help to improve the SM predictions of $K \to \ell\nu_\ell\ell'^+\ell'^-$ decay width. In the past few years, some rare kaon decays have been studied successfully using lattice QCD, such as $K^+ \to \pi^+\nu\bar{\nu}$ [8–12] and $K \to \pi\ell^+\ell^-$ [13,14]. Besides these, other processes involving both weak and electromagnetic interactions—e.g., the radiative corrections to the leptonic and semileptonic decays—have also been investigated recently [15–24]. It is interesting to have the lattice QCD study extend its horizon to include the $K \to \ell\nu_\ell\ell'^+\ell'^-$ decay, where the final state involves four daughter particles.

Here we find that a direct lattice QCD calculation of the $K \to \ell\nu_\ell\ell'^+\ell'^-$ decay width is encountered with the following technical problems:

(1) General finite-volume effects: In order to calculate the decay width, one needs to know the arbitrary momentum dependence of the decay amplitude. However, through discrete Fourier transformation the lattice data from a finite-volume box can only access discrete momenta. This problem appears as finite-volume effects in the calculation of decay width.

(2) Temporal truncation effects: As is shown in Sec. III, using the hadronic function in coordinate space, we perform an integral in Euclidean time to obtain the hadronic function with an assigned momentum. In the process of $K \to K^*\ell'^+\ell'^- \to \ell\nu_\ell\ell'^+\ell'^-$, the K^* in the intermediate state carries nonzero momentum, and thus the energy of the intermediate state is larger than that of the initial/final state. As a result, the time integral converges when the integral range approaches to infinity. However, in the soft-photon region, where the four-momentum of the electromagnetic current $(E, \vec{P})$ is close to zero, the integral converges very slowly. Since the lattice temporal extent T is finite, we find that the temporal truncation effects are not negligible. An extrapolation to infinitely large time extent is required to achieve a precise calculation.

(3) Complex calculation procedures: The calculation of $K \to \ell\nu_\ell\ell'^+\ell'^-$ decay width is of particular complication, because it involves several form factors and four-body phase-space integral. One needs to construct a reliable and convenient approach to calculate the decay amplitude at arbitrary momenta and perform the phase-space integral.

(4) Specific power-law finite-volume effects associated with $K \to \pi\pi\ell\nu_\ell \to \ell\nu_\ell\ell'^+\ell'^-$: This subprocess is essentially a long-distance process involving multihadrons in the intermediate state. When the momentum of the electromagnetic current is fixed, the corresponding power-law finite-volume effects have been studied first by Ref. [25] using the $K_L - K_S$ mass difference as an example, and later by Ref. [26] for more general cases. When calculating the decay width, the momentum of the electromagnetic current runs over the whole allowed phase-space region, while the finite-volume correction becomes more complicated and still remains an open problem. This situation also happens for the $K \to \mu^+\mu^-$ decay, where two off-shell photons are involved [27].

This work is aimed at solving the first three technical problems, building a convenient calculation procedure, and presenting the lattice results of $K \to \ell\nu_\ell\ell'^+\ell'^-$ decay width. The central part of this paper introduces the following methodologies: (1) a scalar function method to compute the hadronic function, (2) an infinite-volume reconstruction (IVR) method [28] to reduce the unphysical temporal truncation and finite-volume effects, and (3) a convenient phase-space integration method to obtain the decay width.

With these developed methods, we calculate $K \to \ell\nu_\ell\ell'^+\ell'^-$ decay width using a gauge ensemble of $N_f = 2 + 1 + 1$-flavor twisted-mass fermion at the unphysical pion mass $m_\pi = 0.3515(15)$ GeV. The valance strange quark mass is tuned to make the kaon mass $m_K = 0.5057(13)$ GeV close to its physical value. The lattice results of the branching ratios are summarized in Table I and are found to be comparable to experimental measurements and ChPT predictions. Systematic errors of our lattice calculation mainly come from unphysical quark mass, nonzero lattice spacing, and residual finite-volume effects. Calculation at the physical quark mass together with the continuum extrapolation will be included in our future work.[1]

In this paper, we will first introduce in Sec. II the decay amplitude of $K \to \ell\nu_\ell\ell'^+\ell'^-$ in Minkowski space. This part follows Refs. [5,30] and is also a necessary part of lattice calculation. In Sec. III, we will establish a connection between the Minkowski hadronic function and the Euclidean one, and we will give a more detailed description of the computational techniques mentioned above, which is the most central part of this paper. Finally, we present the numerical results in Sec. IV and reach a conclusion in Sec. V.

II. DECAY WIDTH OF $K \to \ell\nu_\ell\ell'^+\ell'^-$

Our program aims at the calculation of the branching ratios of $K \to \ell\nu_\ell\ell'^+\ell'^-$ via

[1]As this paper is under peer review, a parallel lattice study is being performed to compute the decay width based on the extraction of the form factors [29].

TABLE I. Comparison of branching ratios of $\mathrm{Br}[K \to \ell\nu_\ell\ell'^+\ell'^-]$ among our lattice-QCD calculation (at $m_\pi = 352$ MeV), ChPT and experiments. In order to compare results with ChPT, we choose the same cuts $m_{ee} > 140$ MeV as those in Ref. [5], where m_{ee} is the invariant mass of the e^+e^- pair. For decays with ee^+e^-, the cuts are applied to both invariant masses. (The kaon mass m_K used in the lattice calculation is slightly different from the physical kaon mass $m_{K,\mathrm{phy}}$. For the lattice results, we rescale the cuts for m_{ee} as $\frac{m_{ee}}{m_K} > \frac{140\ \mathrm{MeV}}{m_{K,\mathrm{phy}}}$.) The experimental results of $K \to e\nu_e e^+e^-$ and $K \to \mu\nu_\mu e^+e^-$ are the extrapolated values from $m_{ee} > 150$ MeV and 145 MeV to $m_{ee} > 140$ MeV. The extrapolation formulas are given in Ref. [3].

Channels	m_{ee} cuts	Lattice ($m_\pi = 352$ MeV)	ChPT [5]	Experiments
$\mathrm{Br}[K \to e\nu_e e^+e^-]$	140 MeV	$1.77(16) \times 10^{-8}$	3.39×10^{-8}	$2.91(23) \times 10^{-8}$ [3]
$\mathrm{Br}[K \to \mu\nu_\mu e^+e^-]$	140 MeV	$10.59(33) \times 10^{-8}$	8.51×10^{-8}	$7.93(33) \times 10^{-8}$ [3]
$\mathrm{Br}[K \to e\nu_e \mu^+\mu^-]$	⋯	$0.72(5) \times 10^{-8}$	1.12×10^{-8}	$1.72(45) \times 10^{-8}$ [4]
$\mathrm{Br}[K \to \mu\nu_\mu \mu^+\mu^-]$	⋯	$1.45(6) \times 10^{-8}$	1.35×10^{-8}	⋯

$$\mathrm{Br}[K \to \ell\nu_\ell\ell'^+\ell'^-] = \frac{1}{2m_K\Gamma_K}\int d\Phi_4 |\mathcal{M}(K \to \ell\nu_\ell\ell'^+\ell'^-)|^2, \quad (1)$$

where $\Gamma_K = 5.3168(86) \times 10^{-14}$ MeV is the kaon decay width from the Particle Data Group [31].[2] $\mathcal{M}(K \to \ell\nu_\ell\ell'^+\ell'^-)$ is the decay amplitude, and $\int d\Phi_4$ indicates a four-body phase-space integral.

Our approach to calculating the $K \to \ell\nu_\ell\ell'^+\ell'^-$ decay width includes three major steps. The first step is to determine the Minkowski hadronic functions

$$H_M^\nu(q) = \langle 0|J_{W,M}^\nu(0)|K(q)\rangle,$$
$$H_M^{\mu\nu}(p,q) = \int d^4x e^{ip\cdot x}\langle 0|T\{J_{\mathrm{em},M}^\mu(x)J_{W,M}^\nu(0)\}|K(q)\rangle, \quad (2)$$

where the electromagnetic and weak currents in Minkowski space are defined as $J_{\mathrm{em},M}^\mu = \frac{2}{3}\bar{u}\gamma^\mu u - \frac{1}{3}\bar{d}\gamma^\mu d - \frac{1}{3}\bar{s}\gamma^\mu s$ and $J_{W,M}^\nu = \bar{s}\gamma^\nu(1-\gamma_5)u$. $p = (E, \vec{p})$ and $q = (m_K, \vec{0})$ are the Minkowski four-momenta of the electromagnetic current and initial kaon state. We define the parameters ρ_1 and ρ_2 as

$$p^2 = \rho_1 m_K^2, \qquad (q-p)^2 = \rho_2 m_K^2. \quad (3)$$

In a lattice QCD study, the hadronic functions are generally calculated in Euclidean space. The connection between Minkowski and Euclidean hadronic functions is established in Sec. III.

As a second step, the decay amplitude $\mathcal{M}(K \to \ell\nu_\ell\ell'^+\ell'^-)$ is constructed by combining the hadronic function $H_M^{\mu\nu}(p,q)$ with the leptonic factor [5]. Here we target on the determination of the amplitude $\mathcal{M}$ with arbitrary momentum dependence.

As a last step, the decay amplitude is used as an input in the integral [Eq. (1)] to obtain the decay width. The definition of the four-body phase-space integral is provided in Ref. [30], which is originally used for the process of $K \to \ell\bar{\ell}\ell'\bar{\ell}'$. We use the Monte Carlo method to perform the phase-space integration.

A. Hadronic function in Minkowski space

In the continuum theory, the hadronic function $H_M^{\mu\nu}(p,q)$ satisfies the Ward identity [5]

$$p_\mu H_M^{\mu\nu}(p,q) = f_K q^\nu, \quad (4)$$

with f_K being the kaon decay constant. Using the Ward identity, $H_M^{\mu\nu}(p,q)$ can be written in terms of form factors [21] as

$$H_M^{\mu\nu}(p,q) = H_1[p^2 g^{\mu\nu} - p^\mu p^\nu] + H_2[(p\cdot q - p^2)p^\mu - p^2(q-p)^\mu](q-p)^\nu - i\frac{F_V}{m_K}\varepsilon^{\mu\nu\alpha\beta}p_\alpha q_\beta + \frac{F_A}{m_K}[(q\cdot p - p^2)g^{\mu\nu} - (q-p)^\mu p^\nu] + f_K\left[g^{\mu\nu} + \frac{(2q-p)^\mu(q-p)^\nu}{2q\cdot p - p^2}\right]. \quad (5)$$

Using the hadronic function $H_M^\nu(q)$, one can construct the amplitude for the subprocess of $K \to \ell\nu_\ell \to \ell\nu_\ell\ell'^+\ell'^-$, as shown in Fig. 1. Using the hadronic function $H_M^{\mu\nu}(p,q)$, the remaining contribution to the decay amplitude of $K \to \ell\nu_\ell\ell'^+\ell'^-$ can be constructed. For the case of $\ell' = \ell$, the decay amplitude consists of two parts, shown as the "Direct" and "Exchange" diagrams in Fig. 2. For $\ell \neq \ell'$, only the "Direct" diagram contributes.

Here we use the case of $\ell' = \ell$ to introduce the expressions for the decay amplitudes. The four-momenta

[2]Note that we do not calculate the total kaon decay width from the lattice.

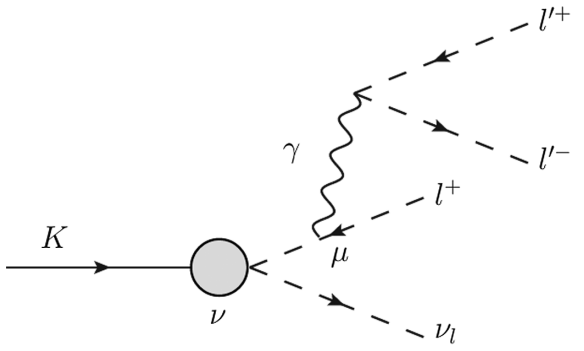

FIG. 1. Contribution of off-shell photon radiation from the final-state lepton in $K \to \ell\nu_\ell\ell'^+\ell'^-$. The hadronic part is described by $H_M^\nu(q)$.

of the final-state leptons are defined as p_i with $i = 1, 2, 3, 4$, as shown in Fig. 2. The decay amplitudes are given as

$$\begin{aligned} i\mathcal{M}_D &= -i\frac{G_F e^2 V_{us}^*}{\sqrt{2}s_{12}}[f_K L^\mu(p_1,p_2,p_3,p_4) \\ &\quad - H_M^{\mu\nu}(p_{12},q)l_\nu(p_3,p_4)][\bar{u}(p_1)\gamma_\mu v(p_2)], \\ i\mathcal{M}_E &= +i\frac{G_F e^2 V_{us}^*}{\sqrt{2}s_{14}}[f_K L^\mu(p_1,p_4,p_3,p_2) \\ &\quad - H_M^{\mu\nu}(p_{14},q)l_\nu(p_3,p_2)][\bar{u}(p_1)\gamma_\mu v(p_4)], \end{aligned} \tag{6}$$

where the terms with a factor of f_K arise from Fig. 1, which has both the "Direct" and the "Exchange" contribution if $l = l'$, and the terms with a factor of $H_M^{\mu\nu}$ come from Fig. 2. Here, $\mathcal{M}_D$ and $\mathcal{M}_E$ stand for the amplitudes from the "Direct" and "Exchange" diagrams, respectively. The photon momentum is given by $p_{ij} \equiv p_i + p_j$, and $s_{ij} \equiv p_{ij}^2$ is the momentum squared. The leptonic factors L^μ and l^μ are defined as

$$\begin{aligned} l^\mu(p_3,p_4) &= \bar{u}(p_3)\gamma^\mu(1-\gamma_5)v(p_4), \\ L^\mu(p_1,p_2,p_3,p_4) &= l^\mu(p_3,p_4) + L'^\mu(p_1,p_2,p_3,p_4), \end{aligned} \tag{7}$$

with

$$\begin{aligned} &L'^\mu(p_1,p_2,p_3,p_4) \\ &\quad = m_\ell \bar{u}(p_3)(1+\gamma_5)\frac{2p_4^\mu + \not{p}_{12}\gamma^\mu}{m_\ell^2 - (p_4+p_{12})^2}v(p_4). \end{aligned} \tag{8}$$

Note that $\bar{u}$ and v in Eqs. (7) and (8) stand for the spinors of ℓ and ν_ℓ, which form a charged weak current, while $\bar{u}$ and v in Eq. (6) stand for the spinors of ℓ^+ and ℓ^- from an electromagnetic current. Finally, V_{us}^* is the CKM matrix element, and G_F is the Fermi constant.

It should be noticed that, the term $f_K g^{\mu\nu}$ in Eq. (5) can produce a contribution proportional to $f_K l^\mu$, which exactly cancels the $f_K l^\mu$ term contained by $f_K L^\mu$ in Eq. (6). We find that the $f_K l^\mu$ term from Fig. 1 would be IR-divergent in the limit of vanishing lepton mass. In order to maintain the exact cancellation in the large IR contribution and reduce the statistical uncertainty, we replace $H_M^{\mu\nu}$ with $H_M'^{\mu\nu}$ in Eq. (6), where $H_M'^{\mu\nu}$ is defined as

$$\begin{aligned} H_M'^{\mu\nu}(p,q) &\equiv H_M^{\mu\nu}(p,q) - f_K g^{\mu\nu} \\ &= H_M^{\mu\nu}(p,q) - \frac{p_\rho H_M^{\rho 0}(p,q)}{m_K}g^{\mu\nu}. \end{aligned} \tag{9}$$

In this way, the amplitudes $\mathcal{M}_D$ and $\mathcal{M}_E$ can be written as

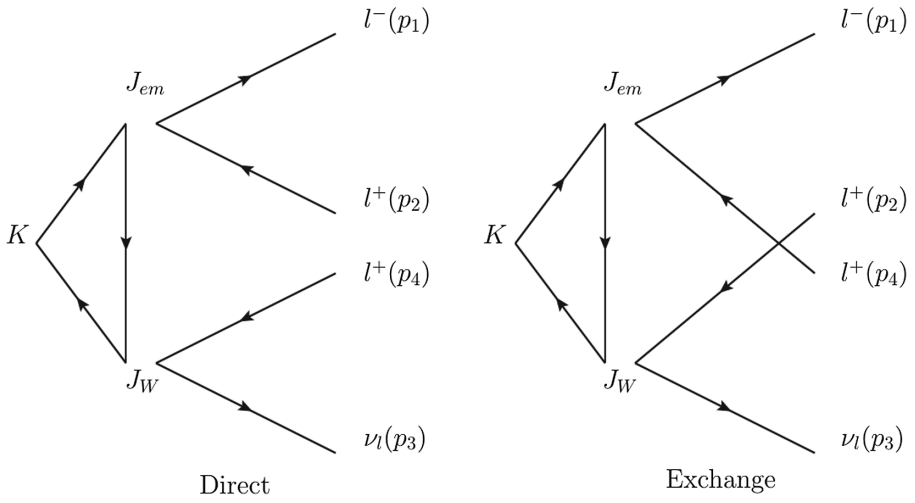

FIG. 2. Contribution of off-shell photon radiation from quarks in $K \to \ell\nu_\ell\ell^+\ell^-$. The hadronic part is described by $H_M^{\mu\nu}(p,q)$.

$$
\begin{aligned}
i\mathcal{M}_D &= -i\frac{G_F e^2 V_{us}^*}{\sqrt{2}s_{12}}[f_K L'^{\mu}(p_1,p_2,p_3,p_4) \\
&\quad - H_M'^{\mu\nu}(p_{12},q)l_\nu(p_3,p_4)][\bar{u}(p_1)\gamma_\mu v(p_2)], \\
i\mathcal{M}_E &= +i\frac{G_F e^2 V_{us}^*}{\sqrt{2}s_{14}}[f_K L'^{\mu}(p_1,p_4,p_3,p_2) \\
&\quad - H_M'^{\mu\nu}(p_{14},q)l_\nu(p_3,p_2)][\bar{u}(p_1)\gamma_\mu v(p_4)].
\end{aligned} \tag{10}
$$

Using $\mathcal{M}_D$ and $\mathcal{M}_E$ as input, the branching ratio of $K \to \ell\nu_\ell\ell'^+\ell'^-$ for $\ell = \ell'$ can be calculated through

$$
\begin{aligned}
&\mathrm{Br}[K \to \ell\nu_\ell\ell^+\ell^-] \\
&= \frac{1}{2m_K\Gamma_K}\int d\Phi_4(|\mathcal{M}_D|^2 + |\mathcal{M}_E|^2 + 2\mathrm{Re}[\mathcal{M}_D\mathcal{M}_E^*]).
\end{aligned} \tag{11}
$$

For $\ell \neq \ell'$, we only have the $|\mathcal{M}_D|^2$ term in the above equation:

$$
\mathrm{Br}[K \to \ell\nu_\ell\ell'^+\ell'^-] = \frac{1}{2m_K\Gamma_K}\int d\Phi_4|\mathcal{M}_D|^2. \tag{12}
$$

B. Phase-space integral

The definition of the four-body phase-space integral follows Ref. [30]. In Ref. [30], the formulas are simplified for the case of the daughter particles with the same masses. Here, we generalize the formulas to the case in which the daughter particles have different masses.

The four-body phase space $d\Phi_4$ is defined as

$$
d\Phi_4 = \frac{\mathcal{S}\lambda m_K^4}{2^{14}\pi^6}dx_{12}dx_{34}dy_{12}dy_{34}d\phi. \tag{13}
$$

Here, $\mathcal{S}$ is a symmetry factor with $\mathcal{S} = 1$ for the case of $\ell \neq \ell'$, and $\mathcal{S} = \frac{1}{2}$ for $\ell = \ell'$. The phase-space variables x_{12}, x_{34}, y_{12}, y_{34}, and ϕ are five independent Lorentz-invariant quantities, with x_{ij} and y_{ij} defined as

$$
\begin{aligned}
x_{12} &= \frac{s_{12}}{m_K^2}, \qquad x_{34} = \frac{s_{34}}{m_K^2}, \\
y_{12} &= \frac{2\bar{p}_{12}\cdot p_{34} - 2p_{12}\cdot p_{34}\delta_{12}}{\lambda m_K^2}, \\
y_{34} &= \frac{2\bar{p}_{34}\cdot p_{12} - 2p_{12}\cdot p_{34}\delta_{34}}{\lambda m_K^2},
\end{aligned} \tag{14}
$$

where $\bar{p}_{ij} \equiv p_i - p_j$, $\lambda \equiv \sqrt{(1-x_{12}-x_{34})^2 - 4x_{12}x_{34}}$, and $\delta_{ij} \equiv \frac{m_i^2 - m_j^2}{s_{ij}}$. The indices 1,2,3,4 specify the particles in the final state. The quantity ϕ can be expressed as

$$
\varepsilon_{\mu\nu\rho\sigma}p_1^\mu p_2^\nu p_3^\rho p_4^\sigma = -\frac{\lambda m_K^4\omega}{16}\sqrt{(\lambda_{12}^2 - y_{12}^2)(\lambda_{34}^2 - y_{34}^2)}\sin\phi, \tag{15}
$$

with

$$
\lambda_{ij} = \sqrt{\left(1 - \frac{m_i^2}{s_{ij}} - \frac{m_j^2}{s_{ij}}\right)^2 - 4\frac{m_i^2 m_j^2}{s_{ij}^2}}, \qquad \omega = 2\sqrt{x_{12}x_{34}}. \tag{16}
$$

To create a Monte Carlo generator, it is useful to assign each particle a four-momentum in the rest frame of the kaon in terms of the phase-space variables as

$$
\begin{aligned}
E_{1(2)} &= m_K\frac{(1+\delta)(1\pm\delta_{12}) \pm \lambda y_{12}}{4}, \\
E_{3(4)} &= m_K\frac{(1-\delta)(1\pm\delta_{34}) \pm \lambda y_{34}}{4}, \\
\vec{p}_{1(2)} &= \mp m_K\sqrt{\frac{x_{12}}{4}(\lambda_{12}^2 - y_{12}^2)}\hat{x} \\
&\quad + m_K\frac{\lambda(1\pm\delta_{12}) \pm (1+\delta)y_{12}}{4}\hat{y}, \\
\vec{p}_{3(4)} &= m_K\sqrt{\frac{x_{34}}{4}(\lambda_{34}^2 - y_{34}^2)}(\mp\cos\phi\hat{x} \pm \sin\phi\hat{z}) \\
&\quad - m_K\frac{\lambda(1\pm\delta_{34}) \pm (1-\delta)y_{34}}{4}\hat{y},
\end{aligned} \tag{17}
$$

with $\delta \equiv x_{12} - x_{34}$. The range of the phase-space variables are adjusted as

$$
\begin{aligned}
&\left(\frac{m_1+m_2}{m_K}\right)^2 \le x_{12} \le \left(1 - \frac{m_3+m_4}{m_K}\right)^2, \\
&\left(\frac{m_3+m_4}{m_K}\right)^2 \le x_{34} \le (1-\sqrt{x_{12}})^2, \\
&-\lambda_{ij} \le y_{ij} \le \lambda_{ij}, \qquad 0 \le \phi \le 2\pi.
\end{aligned} \tag{18}
$$

III. METHODOLOGIES OF LATTICE CALCULATION

The $K \to \ell\nu_\ell\ell'^+\ell'^-$ decay involves several form factors, as given in Eq. (5). The classification of these form factors requires the constraint from the Ward identity. In the lattice calculation, the Ward identity can be easily violated either by the lattice artifacts (e.g., due to the usage of local vector current) or by the finite-volume effects (e.g., due to the usage of the arbitrary momentum). These systematic effects significantly affect the precise determination of the form factors from lattice QCD. Note that our target is to

calculate the total decay width, and the determination of each individual form factor is not a necessary step. In this work, we develop an approach called the *scalar function method*, which provides a convenient way to represent the lattice results for coordinate space matrix elements. Momentum-space matrix elements can be obtained from the scalar function representation with automatic rotational averaging. The IVR method is then applied to make the corrections of the temporal truncation effects and finite-volume effects for the decay amplitude. More details of the methodologies are given as follows.

A. Construction of Minkowski hadronic function using lattice data

In order to reproduce the Minkowski hadronic function using Euclidean lattice data, we shall first establish the relation between the hadronic functions in Euclidean and Minkowski spacetime.

In Euclidean spacetime, the hadronic function is defined as

$$H_E^{\mu\nu}(x) = \langle 0|T\{J^\mu_{\rm em}(x)J^\nu_W(0)\}|K(Q)\rangle, \tag{19}$$

where $Q = (im_K, \vec{0})$ is the Euclidean four-momentum of the initial kaon state. $H_E^{\mu\nu}(x)$ can be extracted from a three-point correlation function, $C^{\mu\nu}(\vec{x}, t; \Delta T)$:

$$C^{\mu\nu}(\vec{x}, t; \Delta T) = \begin{cases} \langle J^\mu_{\rm em}(\vec{x}, t)J^\nu_W(\vec{0}, 0)\phi_K^\dagger(-\Delta T)\rangle, & t \geq 0, \\ \langle J^\mu_W(\vec{0}, 0)J^\nu_{\rm em}(\vec{x}, t)\phi_K^\dagger(t - \Delta T)\rangle, & t < 0. \end{cases} \tag{20}$$

We choose sufficiently large ΔT to guarantee kaon ground-state dominance. Then the hadronic function $H_E^{\mu\nu}(\vec{x}, t)$ can be determined through

$$H^{(L),\mu\nu}_{E,A/V}(\vec{x}, t) = \begin{cases} N_K^{-1}Z_V Z_{A/V} e^{m_K \Delta T} C^{\mu\nu}_{A/V}(\vec{x}, t, \Delta T), & t \geq 0, \\ N_K^{-1}Z_V Z_{A/V} e^{m_K(\Delta T - t)} C^{\mu\nu}_{A/V}(\vec{x}, t, \Delta T), & t < 0. \end{cases} \tag{21}$$

In Eq. (21), we have separated the weak current into axial-vector-current and vector-current parts by using the subscript A/V. Z_A and Z_V are the corresponding renormalization factors. We use the superscript (L) to emphasize that this hadronic function is calculated in the finite volume. The normalization factor $N_K = \langle K|\phi_K^\dagger(0)|0\rangle/(2m_K)$ and the kaon mass m_K can be calculated from the lattice two-point functions.

For simplicity, let us first consider the infinite-volume Euclidean hadronic function $H_E^{\mu\nu}(x)$. In momentum space, it is given by

$$H_E^{\mu\nu}(P, Q) = -i\int_{-T/2}^{T/2} dt \int d^3\vec{x} e^{Et - i\vec{p}\cdot\vec{x}} H_E^{\mu\nu}(x) \tag{22}$$

with the Euclidean momenta

$$P = (iE, \vec{p}), \quad -P^2 = \rho_1 m_K^2, \quad -(Q - P)^2 = \rho_2 m_K^2. \tag{23}$$

In order to calculate decay width, the Euclidean function $H_E^{\mu\nu}(P, Q)$ should be related to the Minkowski one $H_M^{\mu\nu}(p, q)$, which is defined in Sec. II. This relation can be established by inserting the complete set of intermediate states into $H_M^{\mu\nu}(p, q)$ through

$$\begin{aligned} H_M^{\mu\nu}(p, q) &= \int_0^\infty dt \sum_n \langle 0|J^\mu_{{\rm em},M}(0)|n(\vec{p})\rangle_M \langle n(\vec{p})|J^\nu_{W,M}(0)|K(q)\rangle_M e^{i(E - E_n + i\epsilon)t} \\ &\quad + \int_{-\infty}^0 dt \sum_{n_s} \langle 0|J^\nu_{W,M}(0)|n_s(-\vec{p})\rangle_M \langle n_s(-\vec{p})|J^\mu_{{\rm em},M}(0)|K(q)\rangle_M e^{i(E + E_{n_s} - m_K - i\epsilon)t} \\ &= i\sum_n \frac{1}{E - E_n + i\epsilon} \langle 0|J^\mu_{{\rm em},M}(0)|n(\vec{p})\rangle_M \langle n(\vec{p})|J^\nu_{W,M}(0)|K(q)\rangle_M \\ &\quad - i\sum_{n_s} \frac{1}{E + E_{n_s} - m_K - i\epsilon} \langle 0|J^\nu_{W,M}(0)|n_s(-\vec{p})\rangle_M \langle n_s(-\vec{p})|J^\mu_{{\rm em},M}(0)|K(q)\rangle_M. \end{aligned} \tag{24}$$

For $t > 0$ and $t < 0$, the intermediate states are denoted as the state $|n\rangle$ with strangeness $S = 0$ and the state $|n_s\rangle$ with $S = 1$, respectively. The matrix elements $\langle\cdots\rangle_M$ carry a subscript M, which reminds us that they are defined in Minkowski space. The low-lying states for $|n\rangle$ are given by the p-wave $\pi\pi$ states, which couple to the ρ resonance. The lowest state for $|n_s\rangle$ is given by the $|K\rangle$ state. The relevant diagrams for these low-lying states are shown in Figs. 3 and 4.

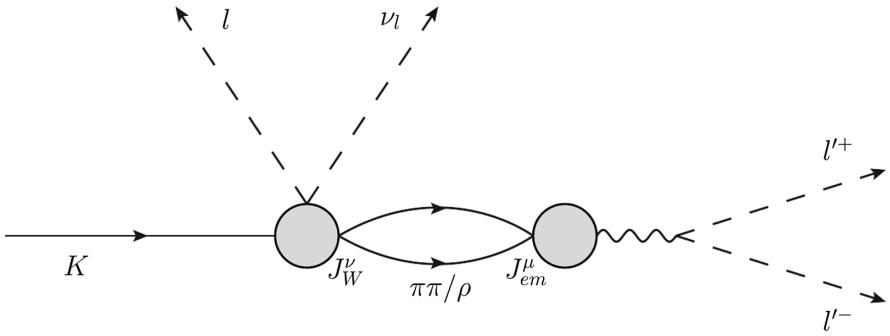

FIG. 3. Low-lying-state dominance for $t > 0$: $\pi\pi$ or ρ states.

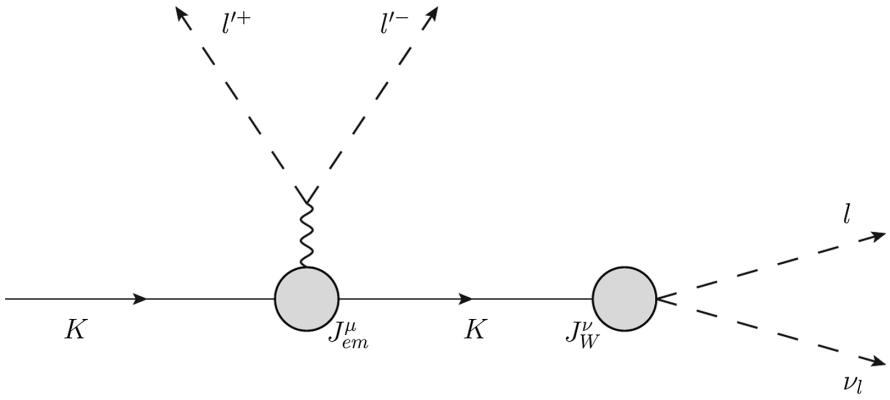

FIG. 4. Low-lying-state dominance for $t < 0$: kaon states.

When inserting the complete set of intermediate states into the Euclidean function $H_E^{\mu\nu}(P,Q)$, we have

$$\begin{aligned} H_E^{\mu\nu}(P,Q) &= -i\int_0^{T/2} dt \sum_n \langle 0|J^\mu_{\rm em}(0)|n\rangle_E \langle n|J^\nu_W(0)|K(Q)\rangle_E e^{(E-E_n)t} \\ &\quad - i\int_{-T/2}^{0} dt \sum_{n_s} \langle 0|J^\nu_W(0)|n_s\rangle_E \langle n_s|J^\mu_{\rm em}(0)|K(Q)\rangle_E e^{(E+E_{n_s}-m_K)t} \\ &= i\sum_n \frac{1-e^{-(E_n-E)T/2}}{E-E_n} \langle 0|J^\mu_{\rm em}(0)|n\rangle_E \langle n|J^\nu_W(0)|K(Q)\rangle_E \\ &\quad - i\sum_{n_s} \frac{1-e^{-(E+E_{n_s}-m_K)T/2}}{E+E_{n_s}-m_K} \langle 0|J^\nu_W(0)|n_s\rangle_E \langle n_s|J^\mu_{\rm em}(0)|K(Q)\rangle_E. \end{aligned} \tag{25}$$

Differently from the Minkowski expression, we have introduced a time integral range $[-T/2, T/2]$ to define the Euclidean hadronic function. This is because the state n consists of a continuous set of $\pi\pi$ states. When $E_n = E_{\pi\pi} < E$, the factor $e^{-(E_n-E)T/2}$ exponentially grows as T increases. In this case, one needs to use the finite-volume hadronic function $H_E^{(L),\mu\nu}(P,Q)$, where the low-lying $\pi\pi$ states are discrete. When a spatial momentum $\vec{p}$ is assigned, one can remove the exponential factor of $e^{-(E_n-E)T/2}$ by isolating each low-lying $\pi\pi$ state. After that, the difference between $H_E^{(L),\mu\nu}(P,Q)$ and the real part of $H_M^{\mu\nu}(p,q)$ can be taken into account by the finite-volume correction formula developed in Refs. [25,26]. The imaginary part of $H_M^{\mu\nu}(p,q)$ can be reproduced by calculating the on-shell decay amplitudes $K \to \pi\pi\ell\nu$ and $\gamma^* \to \pi\pi$, where the finite-volume technique is mature [32,33]. The timelike pion form factor from $\gamma^* \to \pi\pi$ has been calculated on lattice since 2014 [34–36].

In this study, we perform the calculation at the unphysical pion mass $m_\pi = 0.3515(15)$ GeV. As a result, $E_{\pi\pi} - E$ is always larger than zero. In this case, one could take the limit of $T \to \infty$ and establish the relation between

Euclidean and Minkowski matrix elements. Due to the different convention for the J^μ operator,

$$\langle A|J^\mu(0)|B\rangle_M \propto (p_A^\mu \pm p_B^\mu), \qquad p^\mu = (p^0, \vec{p}),$$
$$\langle A|J^\mu(0)|B\rangle_E \propto (P_A^\mu \pm P_B^\mu), \qquad P^\mu = (ip^0, \vec{p}), \tag{26}$$

where J^μ can be either electromagnetic or weak current, one can verify that

$$H_E^{\mu\nu}(P,Q)|_{T\to\infty} = c^{\mu\nu} H_M^{\mu\nu}(p,q) \tag{27}$$

with $c^{00} = -1$, $c^{0i} = c^{i0} = i$, and $c^{ij} = 1$. Thus, we have shown that the Minkowski hadronic function can be calculated by Euclidean lattice data.

B. Scalar function method

In the following part of the paper, for simplicity we will omit the subscript E in the Euclidean hadronic function and use $H^{\mu\nu}(x)$ and $H^{\mu\nu}(P,Q)$ to replace $H_E^{\mu\nu}(x)$, $H_E^{\mu\nu}(P,Q)$. It is straightforward to compute $H^{\mu\nu}(P,Q)$ using the 4×4 Lorentz tensor $H^{\mu\nu}(x)$ as input:

$$H^{\mu\nu}(P,Q) = -i\int_{-T/2}^{T/2} dt \int d^3\vec{x} e^{Et - i\vec{p}\cdot\vec{x}} H^{\mu\nu}(x). \tag{28}$$

We call this the *direct method*.

In a realistic lattice calculation, $H^{\mu\nu}(x)$ is given by the finite-volume lattice data $H^{(L),\mu\nu}(x)$. The data depend on $L^3\times T$ spacetime coordinates, 4×4 Lorentz indices, and two types of current insertions (V/A). Taking a $24^3\times 48$ lattice as an example, the data size is about 650 MB per configuration, as shown in Table II. The computation of the decay width requires integration using $H^{(L),\mu\nu}(x)$ as input and is thus quite complicated.

In this work, we propose to use the scalar function method, which could significantly reduce the size of data input and provide automatic rotational averaging.

TABLE II. Comparison of the size of input data required by the scalar function method and the direct method. By using the scalar function method, the hadronic function $H^{\mu\nu}(x)$ is converted into six scalar functions $I_i(|\vec{x}|^2,t)$. The former requires the total data size of $L^3\times T\times 4\times 4\times 2$, while the latter only requires $r_{\max}^2\times T\times 6$, with $r_{\max}^2 \equiv 3(L/2)^2$. As the lattice size L increases, the scalar function method becomes more efficient compared the direct method.

Method	Direct method	Scalar function method
Stored data	$H^{(L),\mu\nu}(x)$	$I_i^{(L)}(\vec{x}\|^2,t)$
Space-time dimensions	$(L,L,L,T):24^3\times 48$	$(r_{\max}^2,T):432\times 48$
Other dimensions	$(\mu,\nu,V/A):4\times 4\times 2$	6
Data size	≈650 MB/conf	≈2 MB/conf

This simplification can be achieved by converting $H^{\mu\nu}(P,Q)$ and $H^{\mu\nu}(x)$ into the Lorentz scalar functions. For example, $H^{\mu\nu}(P,Q)$ can be used to construct the following Lorentz-invariant quantities:

$$\begin{aligned}
\tilde{I}_1(\rho_1,\rho_2) &= -\delta^{\mu\nu} m_K^2 H^{\mu\nu}(P,Q),\\
\tilde{I}_2(\rho_1,\rho_2) &= Q^\mu Q^\nu H^{\mu\nu}(P,Q),\\
\tilde{I}_3(\rho_1,\rho_2) &= P^\mu Q^\nu H^{\mu\nu}(P,Q),\\
\tilde{I}_4(\rho_1,\rho_2) &= Q^\mu P^\nu H^{\mu\nu}(P,Q),\\
\tilde{I}_5(\rho_1,\rho_2) &= P^\mu P^\nu H^{\mu\nu}(P,Q),\\
\tilde{I}_6(\rho_1,\rho_2) &= \epsilon^{\mu\nu\alpha\beta} P^\alpha Q^\beta H^{\mu\nu}(P,Q).
\end{aligned} \tag{29}$$

Since the momentum Q satisfies the on-shell condition $Q^2 = -m_K^2$, the quantities $\tilde{I}_i(\rho_1,\rho_2)$ only depend on two variables ρ_1 and ρ_2, which are defined in Eq. (23). Then we can write $H^{\mu\nu}(P,Q)$ as a combination of

$$H^{\mu\nu}(P,Q) = \sum_{i=1}^{6} \tilde{w}_i^{\mu\nu}(P,Q)\tilde{I}_i(\rho_1,\rho_2), \tag{30}$$

where $\tilde{w}_i^{\mu\nu}(P,Q)$ are analytically known Lorentz factors. The way to obtain $\tilde{w}_i^{\mu\nu}(P,Q)$ has been discussed in Appendix A.

For $H^{\mu\nu}(x)$, we can also write them in terms of Lorentz-invariant quantities through

$$H^{\mu\nu}(x) = \sum_{i=1}^{6} w_i^{\mu\nu}(x) I_i(|\vec{x}|^2,t), \tag{31}$$

where the I_i's are defined as

$$\begin{aligned}
I_1(|\vec{x}|^2,t) &= \delta^{\mu\nu} H^{\mu\nu}(x),\\
I_2(|\vec{x}|^2,t) &= -\frac{Q^\mu Q^\nu}{m_K^2} H^{\mu\nu}(x) = H^{00}(x),\\
I_3(|\vec{x}|^2,t) &= \frac{x^\mu Q^\nu}{im_K} H^{\mu\nu}(x) - \frac{x\cdot Q}{im_K} I_2 = x^i H^{i0}(x),\\
I_4(|\vec{x}|^2,t) &= x^i H^{0i}(x),\\
I_5(|\vec{x}|^2,t) &= x^\mu x^\nu H^{\mu\nu}(x) - \frac{x\cdot Q}{im_K}(I_3+I_4) - \left(\frac{x\cdot Q}{im_K}\right)^2 I_2\\
&= x^i x^j H^{ij}(x),\\
I_6(|\vec{x}|^2,t) &= \epsilon^{\mu\nu\alpha 0} x^\alpha H^{\mu\nu}(x).
\end{aligned} \tag{32}$$

It is more convenient to write I_i as the functions of the variables $(|\vec{x}|^2,t) = (x^2 - (x\cdot Q)^2/(im_K)^2, (x\cdot Q)/(im_K))$. Again, $w_i^{\mu\nu}(x)$ are also the known factors. The choice of the scalar functions is not unique. Here, we design the scalar functions using the simple combination of x^μ and $H^{\mu\nu}(x)$.

We then put Eqs. (29) and (32) into Eq. (28) and obtain a relation between $I_j(|\vec{x}|^2,t)$ and $\tilde{I}_i(\rho_1,\rho_2)$:

$$\tilde{I}_i(\rho_1,\rho_2) = \int d^4x \phi_{ij}(\rho_1,\rho_2;|\vec{x}|^2,t) I_j(|\vec{x}|^2,t). \quad (33)$$

The detailed expressions for $\phi_{ij}(\rho_1,\rho_2;|\vec{x}|^2,t)$ are given in Appendix A. Note that in $I_j(|\vec{x}|^2,t)$, the index j belongs to $1 \le j \le 6$, $|\vec{x}|^2$ takes values from $[0, r^2_{\max} \equiv 3(L/2)^2]$, and t has the range $[-T/2, T/2]$. Thus, the total data size for $I_j(|\vec{x}|^2,t)$ is accounted as $\sim 6 \times r^2_{\max} \times T$, which is significantly smaller than the size of $H^{\mu\nu}(x)$. A comparison is made in Table II to demonstrate the efficiency of the scalar function method.

Using $I_j(|\vec{x}|^2,t)$ as input and adopting Eqs. (33) and (30), the hadronic function $H^{\mu\nu}(P,Q)$ can be constructed for arbitrary momentum P. Then the decay amplitude $\mathcal{M}(K \to \ell\nu\ell'^+\ell'^-)$ can be determined. Although $I_j(|\vec{x}|^2,t)$ is calculated within a finite-volume and fixed-boundary condition, it only causes the exponentially suppressed finite-volume effects to $\tilde{I}_i(\rho_1,\rho_2)$ due to the cluster decomposition property of QCD.

In the continuum theory $\tilde{I}_i(\rho_1,\rho_2)$ for $i = 1,\ldots 6$ are not fully independent due to the constraint from the Ward identity [Eq. (4)]. As a result, the scalar functions $\tilde{I}_3(\rho_1,\rho_2)$ and $\tilde{I}_5(\rho_1,\rho_2)$ are both proportional to the decay constant f_K as

$$\tilde{I}_3(\rho_1,\rho_2) = P^\mu Q^\nu H^{\mu\nu}(P,Q) = m_K^2 f_K,$$
$$\tilde{I}_5(\rho_1,\rho_2) = P^\mu P^\nu H^{\mu\nu}(P,Q) = \frac{1+\rho_1-\rho_2}{2} m_K^2 f_K. \quad (34)$$

One can either use both $\tilde{I}_3(\rho_1,\rho_2)$ and $\tilde{I}_5(\rho_1,\rho_2)$ in the calculation, or use one of them by treating the other one as the dependent quantity. [In practice, we replace $\tilde{I}_5(\rho_1,\rho_2)$ with $\tilde{I}_3(\rho_1,\rho_2)$.] In the continuum theory with an infinite volume, the two setups are equivalent. On the lattice, the results may disagree due to the violation of the Ward identity by both lattice artifacts and finite-volume effects. In Sec. IV B, we calculate the branching ratios using both setups (denoted as "not using Ward-identity constraint" and "using Ward-identity constraint," respectively) and get consistent results.

C. IVR method

When utilizing Eq. (28) to calculate $H^{\mu\nu}(P,Q)$ on lattice, it shall be pointed out that $H^{\mu\nu}(x)$ needs to be replaced by the finite-volume lattice data $H^{(L),\mu\nu}(x)$. As the lattice simulation is performed with a finite temporal extent T and spatial extent L, the replacement will cause temporal truncation effects and finite-volume effects.

In this section, we will use the IVR method [28,37] to perform the correction for both temporal truncation and finite-volume effects. The idea of the IVR method is that "infinite-volume data" $H^{\mu\nu}(x)$ can be reconstructed from the finite-volume lattice data $H^{(L),\mu\nu}(x)$. This method has been successfully applied to various calculations such as neutrinoless double beta decay [38], pion charge radius [39], radiative decays [40], and two-photon exchange contributions [41]. In this work, the IVR method is separated into two steps, namely IVR and δ_{IVR}. The former mainly corrects the temporal truncation effects, and the latter focuses on the finite-volume effects.

For simplicity, we will discuss IVR techniques using $H^{\mu\nu}(x)$ and $H^{\mu\nu}(P,Q)$, and leave IVR formulas for the scalar functions $I_i(|\vec{x}|^2,t)$ and $\tilde{I}_i(\rho_1,\rho_2)$ in Appendix A. It should be noted that the formulas in Appendix A are what we have actually used in the numerical calculation.

1. Temporal truncation effects

We start the discussion with the temporal truncation effects. As shown in Eq. (25), when the temporal extent T increases, the unphysical terms either exponentially decrease or increase depending on the energy difference between the intermediate states and the initial/final state. Since these unphysical effects are dominated by the ground-state contributions as shown in Figs. 3 and 4, here we only consider the low-lying states $|n\rangle = |\pi\pi(I=L=1)\rangle$ for $t > 0$ and $|n_s\rangle = |K\rangle$ for $t < 0$.

For $t > 0$, since we use the gauge ensemble with $m_\pi = 0.3515(15)$ GeV and $m_K = 0.5057(13)$ GeV, $\pi\pi$ states are always heavier than the kaon state. In our numerical study, we do not observe any statistically significant temporal truncation effects, and the unphysical contribution from $e^{-(E_{\pi\pi}-E)T/2}$ can be safely neglected.

For $t < 0$, the temporal truncation effects are not negligible, especially in the soft photon region, where the electromagnetic current carries vanishing momentum $P = (iE, \vec{p}) \approx (0,\vec{0})$. As a result, the intermediate kaon state has an energy E_K very close to the energy of the initial state m_K. A very large T is required to make the factor $e^{-(E+E_K-m_K)T/2}$ sufficiently small. Unfortunately, this requirement is not satisfied by a typical lattice temporal extent of a few femtometers. Thus, the exponential term $e^{-(E+E_K-m_K)T/2}$ is far from convergence, leading to a large temporal truncation effect.

In our numerical calculation, we find that even beyond the soft photon region, the temporal truncation effects are generally not negligible. This means that we need a systematic improved method to reduce the unphysical contamination from $e^{-(E+E_K-m_K)T/2}$.

2. Finite-volume effects

As explained in Ref. [28], the size of the hadronic function $H^{\mu\nu}(x)$ is exponentially suppressed at large spatial separation $|\vec{x}|$. The rate of suppression depends on the energy difference between the intermediate state and the initial state. If $H^{\mu\nu}(x)$ does not decrease to zero at the boundary of the lattice, then the finite-volume effects are expected to be non-negligible. In other words, the lattice

data $H^{(L),\mu\nu}(x)$ could deviate from the infinite-volume $H^{\mu\nu}(x)$ by a sizable difference. These finite-volume effects propagate into $H^{\mu\nu}(P,Q)$ and are more enhanced when P is a nonlattice momentum.

After this explanation of the origin of both temporal truncation and finite-volume effects, we will start to describe the IVR method to reduce these unphysical systematic effects.

3. Step 1: IVR

In the $t<0$ region, the hadronic function $H^{\mu\nu}(\vec{x},t)$ is saturated by the single-particle states at sufficiently large $|t|$. We indicate such time separation as $|t|>t_s$. For $t\le -t_s$, the hadronic function can be given by

$$\begin{aligned} H^{\mu\nu}(\vec{x},t)|_{t\le -t_s} &= \langle 0|J_A^\nu(\vec{0},0)J_{\rm em}^\mu(\vec{x},t)|K\rangle \\ &= \int \frac{d^3p_K}{(2\pi)^3 2E_K}\langle 0|J_A^\nu(\vec{0},0)|K(p_K)\rangle \\ &\quad\times\langle K(p_K)|J_{\rm em}^\mu(\vec{0},0)|K\rangle e^{-i\vec{p}_K\cdot\vec{x}}e^{(E_K-m_K)t} \\ &= \int \frac{d^3p_K}{(2\pi)^3}\tilde{H}^{\mu\nu}(\vec{p}_K,E_K)e^{-i\vec{p}_K\cdot\vec{x}}e^{(E_K-m_K)t}, \end{aligned} \tag{35}$$

with $\tilde{H}^{\mu\nu}(\vec{p}_K,E_K)$ defined as

$$\begin{aligned} \tilde{H}^{\mu\nu}(\vec{p}_K,E_K) &= \frac{1}{2E_K}\langle 0|J_A^\nu(\vec{0},0)|K(p_K)\rangle \\ &\quad\times\langle K(p_K)|J_{\rm em}^\mu(\vec{0},0)|K\rangle. \end{aligned} \tag{36}$$

We can determine $\tilde{H}^{\mu\nu}(\vec{p}_K,E_K)$ using $H^{\mu\nu}(\vec{x},t)$ at $t=-t_s$ as an input:

$$\tilde{H}^{\mu\nu}(\vec{p}_K,E_K)=\int d^3x' H^{\mu\nu}(\vec{x}',-t_s)e^{i\vec{p}_K\cdot\vec{x}'}e^{(E_K-m_K)t_s}. \tag{37}$$

Using the expression of $\tilde{H}^{\mu\nu}(\vec{p}_K,E_K)$ in Eq. (37), the entire hadronic function $H^{\mu\nu}(\vec{x},t)$ with $t<-t_s$ can be reconstructed via

$$\begin{aligned} &H^{\mu\nu}(\vec{x},t)|_{t\le -t_s} \\ &= \int \frac{d^3p_K}{(2\pi)^3}\tilde{H}^{\mu\nu}(\vec{p}_K,E_K)e^{-i\vec{p}_K\cdot\vec{x}}e^{(E_K-m_K)t} \\ &= \int \frac{d^3p_K}{(2\pi)^3}\int d^3x' H^{\mu\nu}(\vec{x}',-t_s)e^{i\vec{p}_K\cdot(\vec{x}'-\vec{x})}e^{(E_K-m_K)(t+t_s)}. \end{aligned} \tag{38}$$

As a next step, the time integral [Eq. (28)] with the range $-T/2<t<0$ can be separated into two parts: $-t_s<t<0$ and $-T/2<t<-t_s$. We can extend the lower bound of the integral from $-T/2$ to $-\infty$. By putting Eq. (38) into the integral, we have

$$\begin{aligned} &\int_{-\infty}^0 dt\int d^3\vec{x}e^{Et-i\vec{p}\cdot\vec{x}}H^{\mu\nu}(\vec{x},t) \\ &= \int_{-t_s}^0 dt\int d^3\vec{x}e^{Et-i\vec{p}\cdot\vec{x}}H^{\mu\nu}(\vec{x},t) \\ &\quad+\int_{-\infty}^{-t_s} dt\int d^3\vec{x}e^{Et-i\vec{p}\cdot\vec{x}}H^{\mu\nu}(\vec{x},t) \\ &= \int_{-t_s}^0 dt\int d^3\vec{x}e^{Et-i\vec{p}\cdot\vec{x}}H^{\mu\nu}(\vec{x},t) \\ &\quad+\int d^3\vec{x}e^{-i\vec{p}\cdot\vec{x}}H^{\mu\nu}(\vec{x},-t_s)\frac{e^{-Et_s}}{E+E_K-m_K}. \end{aligned} \tag{39}$$

From the second to the third line, the hadronic function $H^{\mu\nu}(\vec{x},t)$ with $t<-t_s$ is reconstructed using Eq. (38). Using the hadronic function at some modest value of t_s allows us to perform the time integral analytically in the whole region of $-\infty<t<-t_s$. Thus, the temporal truncation effects naturally disappear.

In the practical calculation, we use the IVR method to reconstruct the scalar functions $\tilde{I}_i(\rho_1,\rho_2)$. The treatment is very similar to that described above. We separate the time integral into a short-distance part with $t>-t_s$ and a long-distance part with $t<-t_s$, and we obtain $\tilde{I}_i^{(s)}(\rho_1,\rho_2)$ and $\tilde{I}_i^{(\ell)}(\rho_1,\rho_2)$ correspondingly. The total contribution is a combination of

$$\tilde{I}_i^{\rm IVR}(\rho_1,\rho_2)=\tilde{I}_i^{(s)}(\rho_1,\rho_2)+\tilde{I}_i^{(l)}(\rho_1,\rho_2),\quad i=1,\ldots,6. \tag{40}$$

The detailed expressions for $\tilde{I}_i^{(s)}$ and $\tilde{I}_i^{(l)}$ are given in Appendix A.

4. Step 2: $\delta_{\rm IVR}$

After making correction to the temporal truncation effects, the lattice results are still affected by the finite-volume effects, which are denoted as $\delta_{\rm IVR}$ here. In Ref. [28], such correction has been demonstrated to be exponentially suppressed as the lattice size L increases. This exponential behavior is also confirmed by our numerical analysis in Sec. IV. We can calculate and correct the leading effect of this already exponentially suppressed finite-volume error. Although exponentially suppressed, $\delta_{\rm IVR}$ can still be very large if a relatively small lattice (e.g., $La=2.2$ fm in this calculation) is used.

We first introduce the definition of the correction term $\delta_{\rm IVR}$ as follows. The hadronic function $H^{\mu\nu}(P,Q)$ is calculated using $H^{(L),\mu\nu}(x)$ as an input:

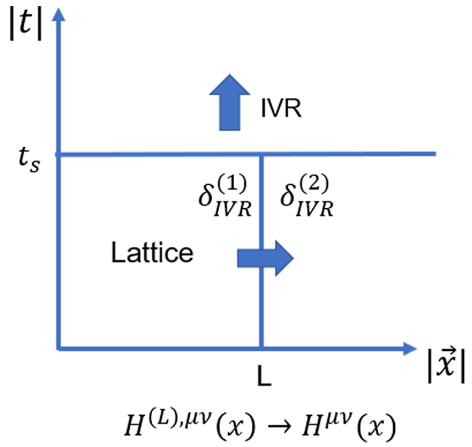

FIG. 5. The main idea of the IVR method. In the temporal direction, $H^{\mu\nu}(x)|_{t<-t_s}$ is reconstructed by using $H^{\mu\nu}(x)$ at $t = -t_s$. In the spatial direction, the finite-volume effects are corrected by calculating $\delta^{(1)}_{\mathrm{IVR}}$ and $\delta^{(2)}_{\mathrm{IVR}}$ via the ground-state dominance.

$$
\begin{aligned}
H^{\mu\nu}(P,Q) &= \int d^4x e^{Et-i\vec{p}\cdot\vec{x}} H^{\mu\nu}(x) \\
&= \int_V d^4x e^{Et-i\vec{p}\cdot\vec{x}} H^{(L),\mu\nu}(x) \\
&\quad + \int_V d^4x e^{Et-i\vec{p}\cdot\vec{x}} (H^{\mu\nu}(x) - H^{(L),\mu\nu}(x)) \\
&\quad + \int_{>V} d^4x e^{Et-i\vec{p}\cdot\vec{x}} H^{\mu\nu}(x). \qquad (41)
\end{aligned}
$$

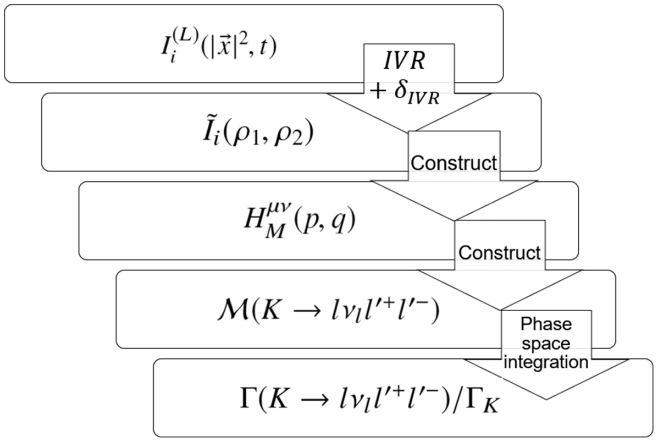

FIG. 7. Lattice calculation procedures of the decay width.

In the above equation, $\int_V d^4x$ indicates that the integral is carried out within a finite spatial volume, while $\int_{>V} d^4x$ means that the integral is performed outside the lattice box in the spatial directions. The second line of Eq. (41) shows the contribution from lattice data $H^{(L),\mu\nu}(x)$. The remaining contributions are given by the third and fourth lines in Eq. (41) and denoted as $\delta^{(1)}_{\mathrm{IVR}}$ and $\delta^{(2)}_{\mathrm{IVR}}$, respectively. Combining $\delta^{(1)}_{\mathrm{IVR}}$ and $\delta^{(2)}_{\mathrm{IVR}}$ together yields the so-called correction δ_{IVR}.

Combining the corrections to the temporal truncation effects and finite-volume effects, the main idea of the IVR method is summarized in Fig. 5.

For sufficiently large time separation, $H^{(L),\mu\nu}(x)$ is saturated by the ground-state contribution:

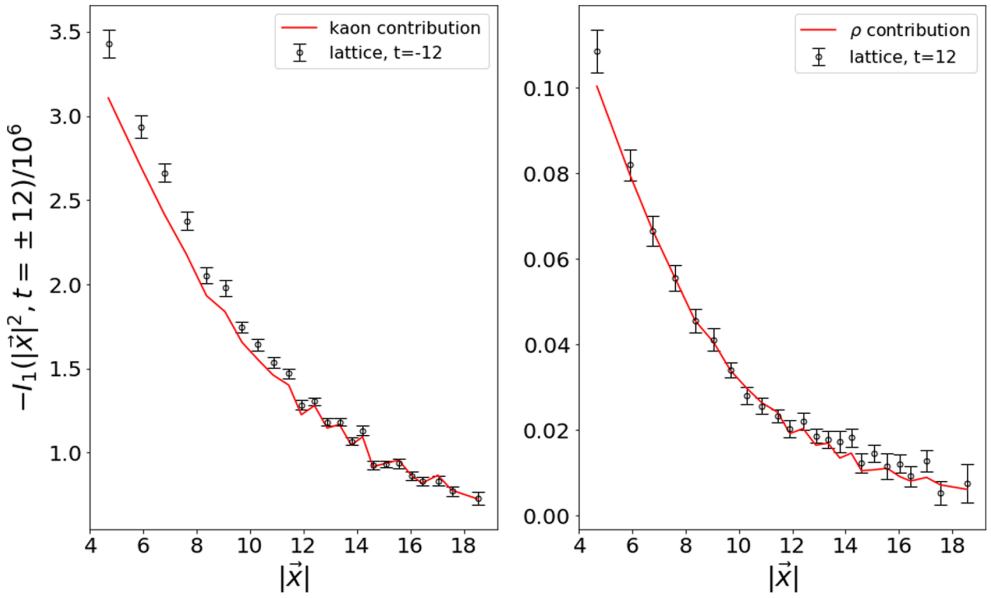

FIG. 6. The comparison between lattice data $I_1(|\vec{x}|^2, t) = \delta^{\mu\nu} H^{\mu\nu}(x)$ and the ground-state contribution. At large $|\vec{x}|$, the lattice data at $t = -12$ and 12 are well dominated by the kaon and ρ states, respectively.

TABLE III. Information of lattice setup.

Label	$L^3 \times T$	a^{-1}	N_{conf}	m_π	m_K	ΔT
cA211b.53.24	$24^3 \times 48$	2.12 GeV	51	0.3515(15) GeV	0.5057(13) GeV	10

$$H^{(L),\mu\nu}(\vec{x}, t < -t_s) = H_K^{(L),\mu\nu}(\vec{x}, t) = \frac{1}{L^3}\sum_{\vec{p}} H_K^{\mu\nu}(\vec{p}, t)e^{i\vec{p}\cdot\vec{x}},$$
$$H^{(L),\mu\nu}(\vec{x}, t > t_s') = H_\rho^{(L),\mu\nu}(\vec{x}, t) = \frac{1}{L^3}\sum_{\vec{p}} H_\rho^{\mu\nu}(\vec{p}, t)e^{i\vec{p}\cdot\vec{x}}. \tag{42}$$

Here, the hadronic kernels $H_{K,\rho}^{\mu\nu}(\vec{p}, t)$ can be written in terms of form factors, whose explicit forms are determined from lattice data $H^{(L),\mu\nu}(\vec{x}, t)$. For more detailed discussions, we refer the reader to Appendix B. In Fig. 6, we show the scalar function $I_1(|\vec{x}|^2, t) = \delta^{\mu\nu}H^{\mu\nu}(x)$ at $t = \pm 12$ as an example that the lattice data are well dominated by the kaon and ρ states. The consistency between lattice data and the ground-state contribution at long distance has also been checked for other scalar functions. As a next step, we reconstruct the infinite-volume hadronic function $H_{K,\rho}^{\mu\nu}(x)$ and calculate the correction δ_{IVR} through

$$\begin{aligned}
\delta_{\text{IVR}} &\approx \delta_{\text{IVR},K} + \delta_{\text{IVR},\rho}, \\
\delta_{\text{IVR},K} &= \int_V d^4x e^{Et-i\vec{p}\cdot\vec{x}}(H_K^{\mu\nu}(x) - H_K^{(L),\mu\nu}(x)) \\
&\quad + \int_{>V} d^4x e^{Et-i\vec{p}\cdot\vec{x}} H_K^{\mu\nu}(x), \\
\delta_{\text{IVR},\rho} &= \int_V d^4x e^{Et-i\vec{p}\cdot\vec{x}}(H_\rho^{\mu\nu}(x) - H_\rho^{(L),\mu\nu}(x)) \\
&\quad + \int_{>V} d^4x e^{Et-i\vec{p}\cdot\vec{x}} H_\rho^{\mu\nu}(x).
\end{aligned} \tag{43}$$

Using the approach described above, we can also apply the finite-volume correction to the scalar functions and obtain

$$\delta_i^{\text{IVR}}(L) \approx \delta_{i,K}^{\text{IVR}}(L) + \delta_{i,\rho}^{\text{IVR}}(L) \tag{44}$$

with

$$\delta_{i,K/\rho}^{\text{IVR}}(L) = \tilde{I}_{i,K/\rho}^{\text{IVR}}(\rho_1, \rho_2) - \tilde{I}_{i,K/\rho}^{\text{IVR}}(\rho_1, \rho_2; L), \tag{45}$$

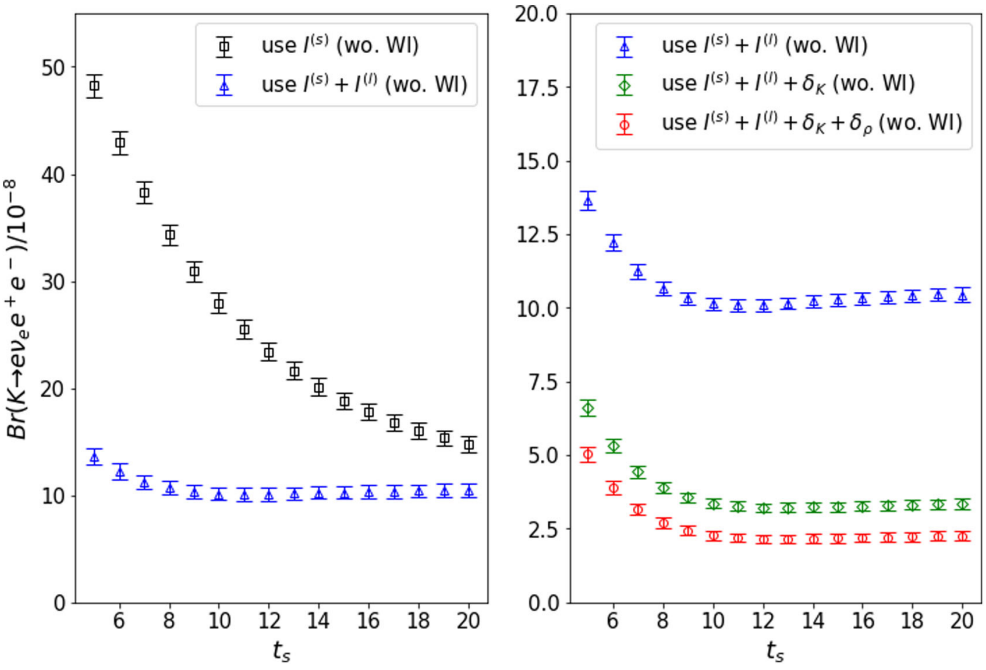

FIG. 8. IVR results for $K \to e\nu_e e^+e^-$ ($L_\infty = 72$). The constraint from the Ward identity is not used here. In the left-hand panel, the data points marked with black squares are compiled using the short-distance contribution $\tilde{I}_i^{(s)}$, while the ones marked with blue triangles use both short-distance and long-distance contributions, namely $\tilde{I}_i^{(s)} + \tilde{I}_i^{(\ell)}$. The right-hand panel shows that the results shift due to corrections from the kaon state $\delta_{i,K}^{\text{IVR}}$ and the ρ state $\delta_{i,\rho}^{\text{IVR}}$.

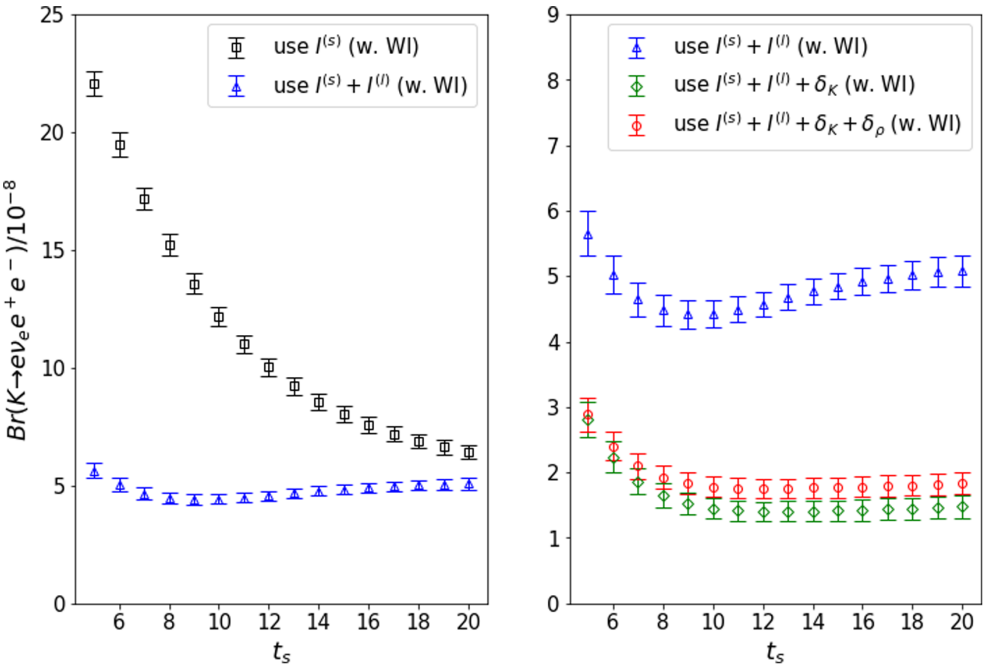

FIG. 9. Similar to Fig. 8, but utilizing the constraint from the Ward identity.

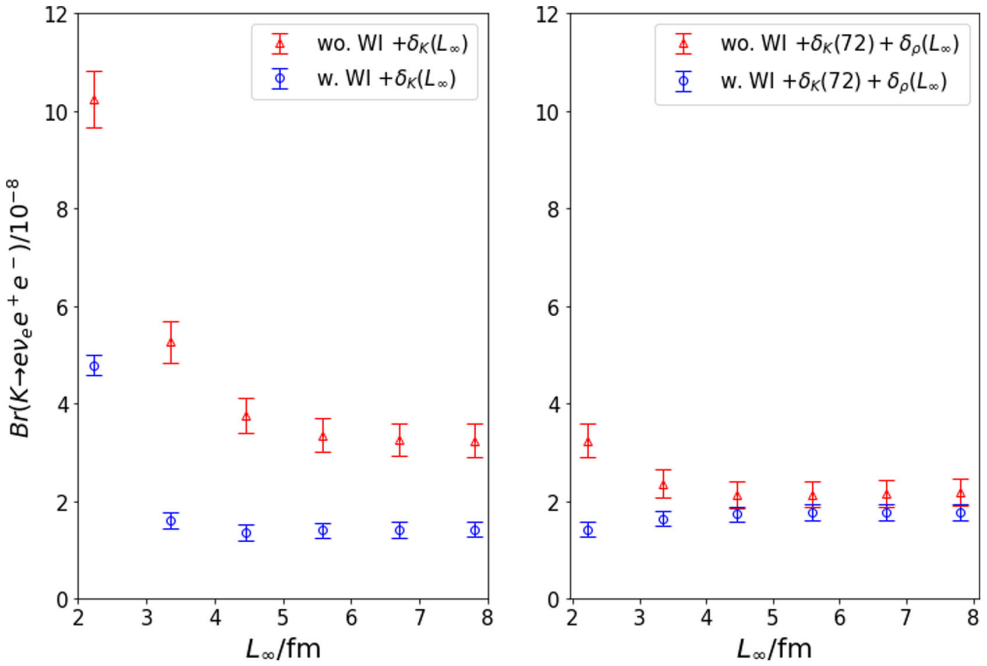

FIG. 10. Examination of L_∞ dependence in the δ_i^{IVR} corrections. Here we use the $K \to e\nu_e e^+ e^-$ decay as an example. In the left-hand panel, we show the finite-volume correction $\delta_{i,K}^{\mathrm{IVR}}$ as a function of L_∞. In the right-hand panel, we fix $\delta_{i,K}^{\mathrm{IVR}}$ at $L_\infty = 72$ and show the correction $\delta_{i,\rho}^{\mathrm{IVR}}$ as a function of L_∞. When $L_\infty = L = 24$ (corresponding to 2.2 fm), no correction is made, and $\delta_{\mathrm{IVR}} = 0$. With increasing L_∞, δ_i^{IVR} exponentially converges, and $L_\infty = 72$ (corresponding to 6.7 fm) is a sufficiently large lattice size to approximate an infinite one.

where the subscript K or ρ is used to indicate the scalar functions compiled from the ground-state contribution. A parameter L is introduced to specify the scalar functions in the finite volume. For scalar functions in the infinite volume, $\tilde{I}^{\mathrm{IVR}}_{i,K/\rho}(\rho_1,\rho_2)$, it can be approximated by $\tilde{I}^{\mathrm{IVR}}_{i,K/\rho}(\rho_1,\rho_2;L_\infty)$ with a sufficiently large L_∞.

D. Computation of the decay width

In this section, we summarize the procedure to compute the decay width of $K\to\ell\nu\ell'^{+}\ell'^{-}$. The outline of the main steps is shown in Fig. 7.

In our calculation, the kaon mass $m_{K,\mathrm{lat}}=0.5057(13)$ GeV is slightly larger than its physical value $m_{K,\mathrm{phy}}=0.493677(16)$ GeV [42]. This affects the decay width in two ways: (1) the m_K dependence of hadronic function, and (2) the change of phase space. In order to reduce the latter, for any dimensional quantities $O^{[n]}$ with dimension n, we rescale them as

$$\bar{O}^{[n]}=O^{[n]}\xi_K^n,\qquad \xi_K\equiv\frac{m_{K,\mathrm{phy}}}{m_{K,\mathrm{lat}}}. \tag{46}$$

For example, the decay constant and the hadronic function are rescaled as

$$\bar{f}_K=\xi_K f_K,\qquad \bar{H}^{\mu\nu}_M(p,q)=\xi_K H^{\mu\nu}_M(p,q), \tag{47}$$

and the decay amplitudes originally defined in Eq. (10) are rescaled as

$$\bar{\mathcal{M}}_D=\xi_K\mathcal{M}_D,\qquad \bar{\mathcal{M}}_E=\xi_K\mathcal{M}_E. \tag{48}$$

As the Fermi constant G_F is a fixed coefficient, $\mathcal{M}_{D,E}$ are considered here as the dimension-one quantities. If there exists a phase-space integral, then $\frac{O^{[n]}}{m^n_{K,\mathrm{lat}}}$ relies on the dimensionless variables $\frac{P^2}{m^2_{K,\mathrm{lat}}}$ and $\frac{P\cdot Q}{m^2_{K,\mathrm{lat}}}$. These variables take the same integral range as the ones in the physical case. We then multiply $\frac{O^{[n]}}{m^n_{K,\mathrm{lat}}}$ by a factor of $m^n_{K,\mathrm{phy}}$ to obtain a dimensional quantity.

For the lattice calculation of $\mathrm{Br}[K\to\ell\nu_\ell\ell'^{+}\ell'^{-}]$ with $\ell=\ell'$, we use the Monte Carlo integration. Within the allowed phase-space range, the five parameters, $(x_{12},x_{34},y_{12},y_{34},\phi)$, are randomly generated N_{MC} times.

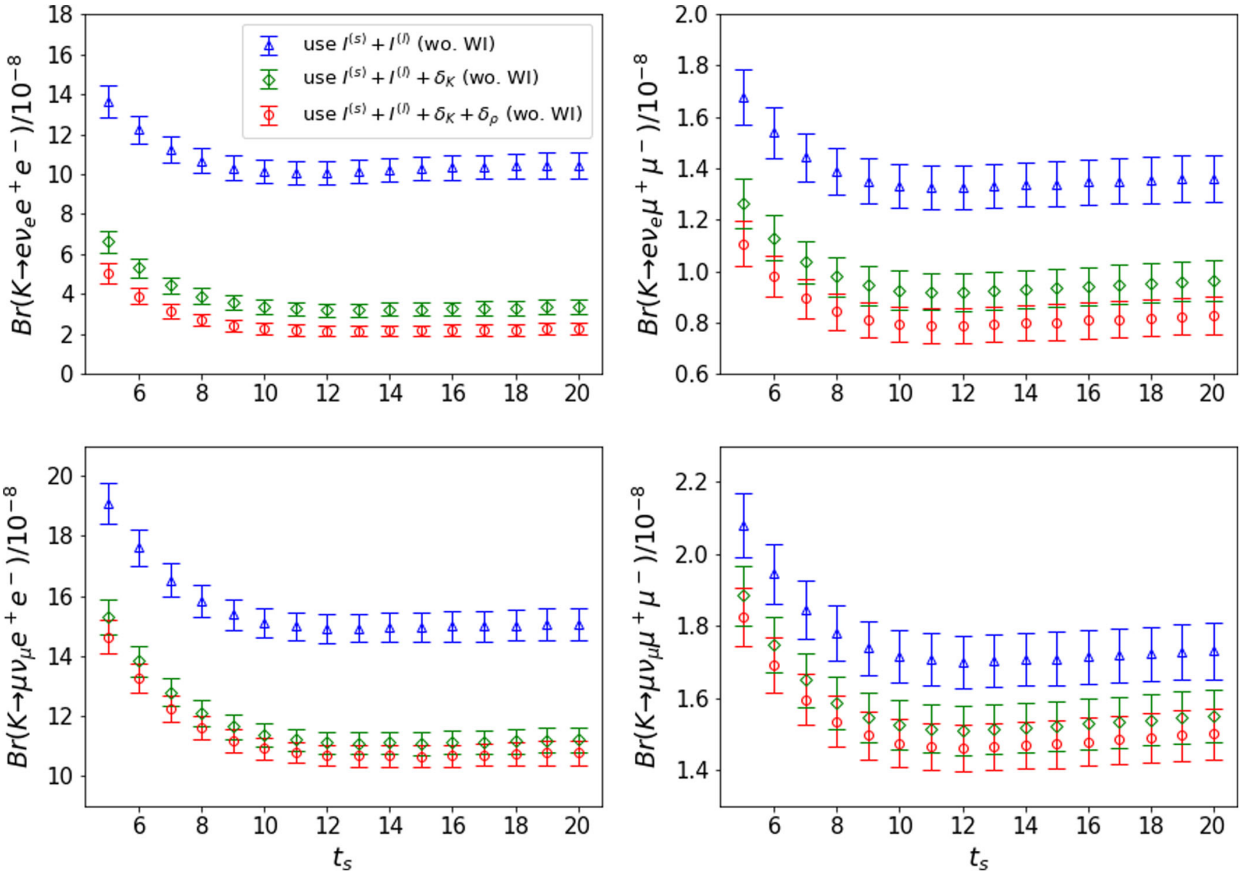

FIG. 11. IVR results for four channels of $K\to\ell\nu_\ell\ell'^{+}\ell'^{-}$. We do not utilize the Ward identity constraint here. The upper-left figure for $K\to e\nu_e e^+e^-$ has been shown in the right-hand panel of Fig. 8. We include it here for the sake of an easier comparison with other three channels. Through this comparison, we find that the $\delta^{\mathrm{IVR}}_{i,K}$ corrections are important for all the channels. The corrections from $\delta^{\mathrm{IVR}}_{i,\rho}$ are less significant but still comparable to the size of the statistical errors.

Given each momentum setup, $\bar{H}_M^{\mu\nu}(p_{12}, q)$ and $\bar{H}_M^{\mu\nu}(p_{14}, q)$ are calculated using the IVR method. In order to get the decay amplitude in Eq. (48), numerical realization of the spinor products is utilized. The branching ratio is calculated as follows:

$$\begin{aligned}
&\mathrm{Br}[K \to l\nu_\ell\ell^+\ell^-] \\
&= \frac{1}{2m_K\Gamma_K}\int d\Phi_4(|\bar{\mathcal{M}}_D|^2 + |\bar{\mathcal{M}}_E|^2 + 2\mathrm{Re}[\bar{\mathcal{M}}_D\bar{\mathcal{M}}_E^*]) \\
&= \frac{1}{2m_K\Gamma_K}\frac{S}{N_{MC}} \\
&\quad\times \sum_{i=1}^{N_{MC}} \frac{\mathcal{S}\lambda m_K^4}{2^{14}\pi^6}(|\bar{\mathcal{M}}_D|^2 + |\bar{\mathcal{M}}_E|^2 + 2\mathrm{Re}[\bar{\mathcal{M}}_D\bar{\mathcal{M}}_E^*])_i, \quad (49)
\end{aligned}$$

where S is the hypervolume of the integration range and $m_K = m_{K,\mathrm{phy}}$.

In the practical calculation, we choose $N_{MC} = 10\,000$, and we confirm that the Monte Carlo error is much less than the statistical error. Considering the fact that the construction of the scalar functions is nontrivial, the Monte Carlo integration thus provides an easily implemented approach to determining the decay width.

IV. NUMERICAL RESULTS

A. Lattice setup

In the lattice calculation, we use a gauge ensemble with an $N_f = 2 + 1 + 1$-flavor twisted-mass fermion generated by the ETM Collaboration [43]. The light quark mass is unphysical, with $m_\pi = 352$ MeV. We tune the valence strange quark mass to have the kaon mass close to its physical value. Parameters of the gauge ensemble are listed in Table III together with the information of ΔT, whose value shall be set sufficiently large to suppress the excited-state contamination.

In order to calculate the hadronic functions, three-point correlation functions are calculated on the lattice. The initial kaon state is created using a Coulomb gauge-fixed wall-source operator. We place two point-source propagators and one wall-source propagator at each time slice and perform a time translation average over all time slices to obtain the three-point function.

B. Results

In Figs. 8 and 9, we take $K \to e\nu_e e^+e^-$ as an example to show the results of the branching ratio as a function of t_s. In the left-hand panels, the black square data points are compiled using the short-distance contribution $\tilde{I}_i^{(s)}$,

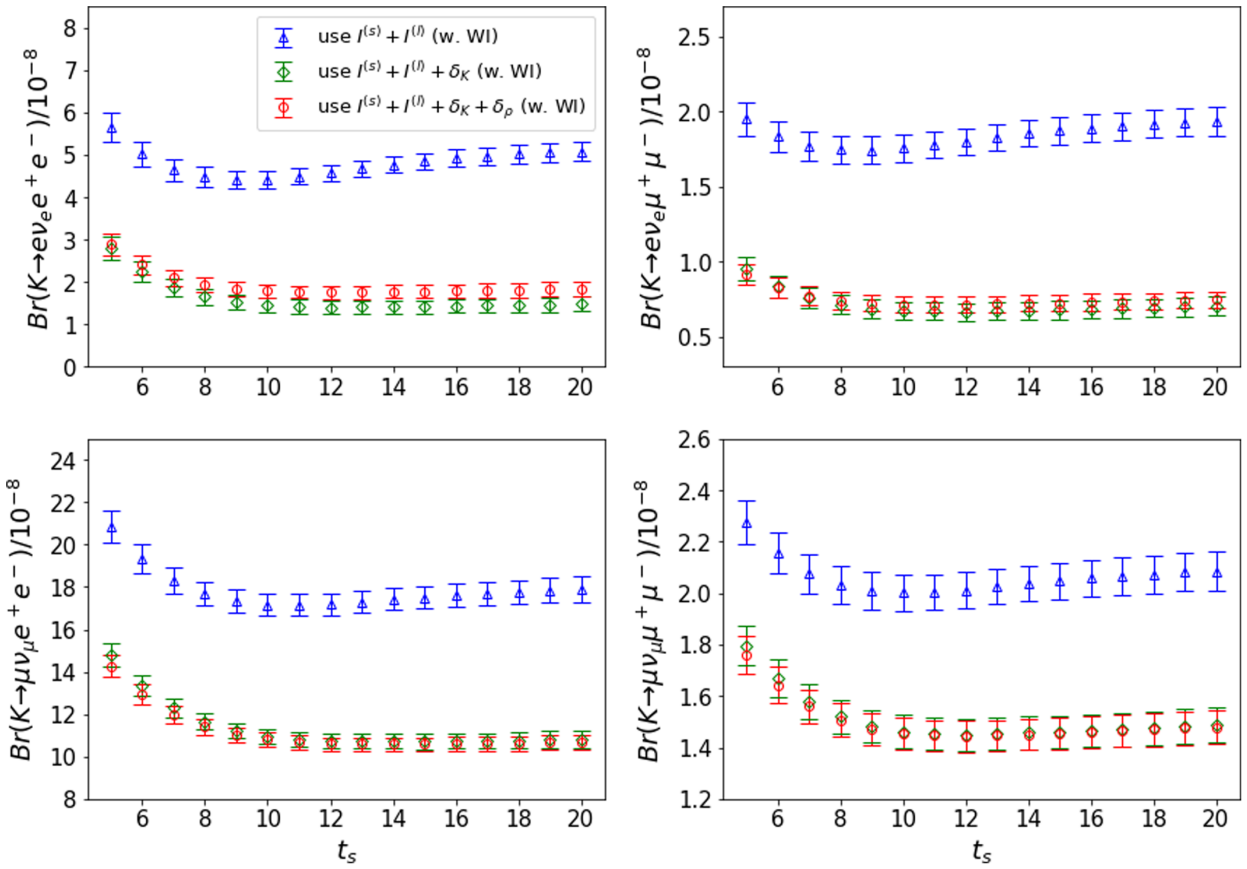

FIG. 12. Similar to Fig. 11, but utilizing the constraint from the Ward identity.

TABLE IV. A comparison of the lattice results when using or not using the constraint from the Ward identity.

Channel	Using Ward identity constraint	Not using Ward identity constraint
$\mathrm{Br}[K \to e\nu_e e^+ e^-]$	$1.77(16) \times 10^{-8}$	$2.18(27) \times 10^{-8}$
$\mathrm{Br}[K \to \mu\nu_\mu e^+ e^-]$	$10.59(33) \times 10^{-8}$	$10.68(36) \times 10^{-8}$
$\mathrm{Br}[K \to e\nu_e \mu^+ \mu^-]$	$0.72(5) \times 10^{-8}$	$0.80(7) \times 10^{-8}$
$\mathrm{Br}[K \to \mu\nu_\mu \mu^+ \mu^-]$	$1.45(6) \times 10^{-8}$	$1.47(7) \times 10^{-8}$

while the blue triangular ones use both short-distance and long-distance contributions. A significant temporal truncation effect is found, demonstrating the importance of the IVR correction. The time t_s needs to be sufficiently large to guarantee the ground-intermediate-state dominance. The figure shows that starting from $t_s \approx 12$, the branching ratio is independent from the choice of t_s.

In the right-hand panels of Figs. 8 and 9, the effects of $\delta^{\mathrm{IVR}}_{i,K}$ and $\delta^{\mathrm{IVR}}_{i,\rho}$ are shown. These corrections are made with the choice of $L_\infty = 72$. We find a large correction from the kaon state and a relatively smaller correction from the ρ state. Given the $L = 2.2$ fm lattice used in our calculation, it is essential to include both corrections.

For the results shown in Figs. 8 and 9, the parameter L_∞ is chosen as $L_\infty = 72$. In Fig. 10, we examine the L_∞ dependence of the results. The left-hand panel shows that the corrections of $\delta^{\mathrm{IVR}}_{i,K}$ become much smaller when using the constraint from the Ward identity. The right-hand panel shows that by including the corrections of $\delta^{\mathrm{IVR}}_{i,\rho}$, the lattice results, whether using or not using the Ward identity constraint, start to converge at large L_∞. We also confirm that as L_∞ increases, the finite-volume effects exponentially suppress, and $L_\infty = 72$ is an appropriate choice to approximate the infinitely large spatial extent.

In Figs. 11 and 12, IVR results for all four channels of $K \to \ell\nu_\ell \ell'^+ \ell'^-$ are shown. The final results of the branching ratio are summarized in Table IV, where we make a comparison between using and not using the constraint from the Ward identity. The results are very consistent. As the former suffers from much smaller finite-volume effects in the $K \to e\nu_e e^+ e^-$ decay, we quote the corresponding results in Table I for a comparison with ChPT and experiments. All the lattice results are compiled using the fitting range $t_s \in [12, 17]$ and including the corrections from both $\delta^{\mathrm{IVR}}_{i,K}$ and $\delta^{\mathrm{IVR}}_{i,\rho}$. We find that the lattice results are comparable to experimental or ChPT ones. The systematic errors of our results mainly come from unphysical quark masses, lattice artifacts, and residual finite-volume effects, which are left for a future study.

V. CONCLUSION

In this work, we build a lattice calculation procedure to determine the $K \to \ell\nu_\ell \ell'^+ \ell'^-$ decay width by solving a series of technical problems. The IVR method is used to reduce temporal truncation effects and finite-volume effects. Other approaches, such as the scalar function method and Monte Carlo phase-space integration, are proposed to simplify the calculation. Using these techniques, a practical methodology is developed to compute the decay width with four daughter particles in the final state, as summarized in Fig. 7.

Using this methodology, we perform a realistic lattice calculation of the $K \to \ell\nu_\ell \ell'^+ \ell'^-$ decay width using an ensemble with pion mass 352 MeV and kaon mass 506 MeV, and we obtain branching ratios comparable to ChPT or experimental results. Through this calculation, we demonstrate the capability of lattice QCD to improve the Standard Model prediction of $K \to \ell\nu_\ell \ell'^+ \ell'^-$ decay width. By examining the t_s dependence and L_∞ dependence of the decay width, we show that the IVR method is a vital approach to reducing the systematic effects. Future work is still required to address the power-law finite-volume effects in the subprocess of $K \to \pi\pi\ell\nu_\ell \to \ell\nu_\ell \ell'^+ \ell'^-$ and make a full control of various systematic effects.

ACKNOWLEDGMENTS

We thank Guido Martinelli for giving an inspiring lecture at the lattice QCD summer school held at Peking University in 2019, which motivates this work. We thank the ETM Collaboration for sharing the gauge configurations with us. X. F. and L. C. J. gratefully acknowledge many helpful discussions with our colleagues from the RBC-UKQCD Collaboration. X. F., X. Y. T., and T. W. are supported in part by NSFC of China under Grants No. 12125501, No. 12070131001, No. 12141501, and No. 11775002, and by the National Key Research and Development Program of China under Contract No. 2020YFA0406400. L. C. J. acknowledges support by DOE Office of Science Early Career Award No. DE-SC0021147 and DOE Grant No. DE-SC0010339. The calculation was carried out on TianHe-3 (prototype) at the Chinese National Supercomputer Center in Tianjin.

APPENDIX A: FORMULAS IN THE SCALAR FUNCTION METHOD

1. Infinite-volume case

In Sec. III, the scalar function method is described by Eqs. (30) and (33). In this section, we will give the detailed expression to calculate $\tilde{I}_i(\rho_1, \rho_2)$ and then discuss the approach to construct $H^{\mu\nu}(P, Q)$ using the scalar functions.

We start with the relation

$$H^{\mu\nu}(P, Q) = -i \int d^4x e^{Et - i\vec{p}\cdot\vec{x}} H^{\mu\nu}(x). \tag{A1}$$

Combining Eq. (A1) with the Lorentz factors given in Eq. (29), we can obtain the relation between $\tilde{I}_i(\rho_1,\rho_2)$ and $I_i(|\vec{x}|^2,t)$. Here we give the detailed expressions of $\tilde{I}_i(\rho_1,\rho_2)$ as

$$\tilde{I}_1(\rho_1,\rho_2) = im_K^2 \int d^4x e^{Et} j_0(\varphi) I_1(|\vec{x}|^2,t), \tag{A2a}$$

$$\tilde{I}_2(\rho_1,\rho_2) = im_K^2 \int d^4x e^{Et} j_0(\varphi) I_2(|\vec{x}|^2,t), \tag{A2b}$$

$$\tilde{I}_3(\rho_1,\rho_2) = im_K E \int d^4x e^{Et} j_0(\varphi) I_2(|\vec{x}|^2,t) - im_K|\vec{p}| \int d^4x e^{Et} \frac{j_1(\varphi)}{|\vec{x}|} I_3(|\vec{x}|^2,t), \tag{A2c}$$

$$\tilde{I}_4(\rho_1,\rho_2) = im_K E \int d^4x e^{Et} j_0(\varphi) I_2(|\vec{x}|^2,t) - im_K|\vec{p}| \int d^4x e^{Et} \frac{j_1(\varphi)}{|\vec{x}|} I_4(|\vec{x}|^2,t), \tag{A2d}$$

$$\begin{aligned}\tilde{I}_5(\rho_1,\rho_2) = {} & iE^2 \int d^4x e^{Et} j_0(\varphi) I_2(|\vec{x}|^2,t) + i|\vec{p}|^2 \int d^4x e^{Et} \frac{j_2(\varphi)}{|\vec{x}|^2} I_5(|\vec{x}|^2,t) \\ & - i|\vec{p}| \int d^4x e^{Et} \frac{j_1(\varphi)}{|\vec{x}|} [EI_3(|\vec{x}|^2,t) + EI_4(|\vec{x}|^2,t) + I_1(|\vec{x}|^2,t) - I_2(|\vec{x}|^2,t)],\end{aligned} \tag{A2e}$$

$$\tilde{I}_6(\rho_1,\rho_2) = -im_K|\vec{p}| \int d^4x e^{Et} \frac{j_1(\varphi)}{|\vec{x}|} I_6(|\vec{x}|^2,t). \tag{A2f}$$

Note that in the continuum theory, the scalar functions $\tilde{I}_i(\rho_1,\rho_2)$ do not depend on the direction of $\vec{p}$. Thus, in the derivation of the above equations we have performed an average over the solid angle of $\vec{p}$. After the average, the factor $e^{-i\vec{p}\cdot\vec{x}}$ is converted into a spherical Bessel function $j_0(\varphi)$, with $\varphi = |\vec{p}||\vec{x}|$. In total, three spherical Bessel functions appear in Eqs. (A2a)–(A2f). They take the standard definition as

$$\begin{aligned} j_0(\varphi) &\equiv \frac{\sin\varphi}{\varphi}, \qquad j_1(\varphi) \equiv \frac{\sin\varphi - \varphi\cos\varphi}{\varphi^2}, \\ j_2(\varphi) &\equiv \frac{(3-\varphi^2)\sin\varphi - 3\varphi\cos\varphi}{\varphi^3}. \end{aligned} \tag{A3}$$

In the numerical calculation, when the variables ρ_1 and ρ_2 are given, the values of $|\vec{p}|$ and E can be determined through

$$\begin{aligned} |\vec{p}| &= \frac{1}{2} m_K \sqrt{(1+\rho_1-\rho_2)^2 - 4\rho_1}, \\ E &= \frac{1}{2} m_K (1+\rho_1-\rho_2). \end{aligned} \tag{A4}$$

Once these scalar functions $\tilde{I}_i(\rho_1,\rho_2)$ are available, $H^{\mu\nu}(P,Q)$ can be easily constructed using Eq. (30). In the numerical calculation, $w_i(P,Q)$ in Eq. (30) is implicitly derived using following procedures:

(1) A general factorization of $H^{\mu\nu}(P,Q)$ is used with

$$\begin{aligned} H^{\mu\nu}(P,Q) = {} & a(\rho_1,\rho_2) P^\mu Q^\nu + b(\rho_1,\rho_2) P^\nu Q^\mu \\ & + c(\rho_1,\rho_2) P^\mu P^\nu + d(\rho_1,\rho_2) Q^\mu Q^\nu \\ & + e(\rho_1,\rho_2) \delta^{\mu\nu} m_K^2 \\ & + f(\rho_1,\rho_2) \epsilon^{\mu\nu\alpha\beta} P^\alpha Q^\beta. \end{aligned} \tag{A5}$$

(2) $\tilde{I}_i(\rho_1,\rho_2)(i=1\ldots6)$ and $a(\rho_1,\rho_2),\ldots,f(\rho_1,\rho_2)$ are related by a simple linear transformation. We can then solve the solution for $a(\rho_1,\rho_2),\ldots,f(\rho_1,\rho_2)$ and construct $H^{\mu\nu}(P,Q)$ using Eq. (A5).

2. Scalar functions with the IVR corrections

In Sec. III, IVR method is proposed to correct the temporal truncation effects and the finite-volume effects for the hadronic functions $H^{\mu\nu}(P,Q)$. In this section, we show how to apply the IVR method to the scalar functions.

We shall point out first that the calculation of $\tilde{I}_6(\rho_1,\rho_2)$ does not require the IVR correction. It is because $\tilde{I}_6(\rho_1,\rho_2)$ is projected out by using the Lorentz factor of $\varepsilon_{\mu\nu\alpha\beta}P^\alpha Q^\beta$. In this quantity, the intermediate states are given by the states heavier than initial kaon state, and thus the temporal truncation effects and finite-volume effects can be neglected.

In the calculation of $\tilde{I}_i(\rho_1,\rho_2)$, with $i=1,\ldots,5$, we also use $t=-t_s$ to separate the time integral into a short-distance part and a long-distance part:

$$\tilde{I}_i(\rho_1,\rho_2) = \tilde{I}_i^{(s)}(\rho_1,\rho_2) + \tilde{I}_i^{(\ell)}(\rho_1,\rho_2). \tag{A6}$$

For the short-distance part, we replace $\tilde{I}_i^{(s)}(\rho_1,\rho_2)$ with the lattice data $\tilde{I}_i^{(s)}(\rho_1,\rho_2,L)$. For the long-distance part, we use the lattice data of $I_i^{(L)}(|\vec{x}|^2,t)$ at $t=-t_s$ as input. Through the kaon-intermediate-state dominance, $\tilde{I}_i^{(\ell)}(\rho_1,\rho_2,L)$ can be reconstructed. The detailed expressions are given as

$$\tilde{I}_1^{(\ell)}(\rho_1,\rho_2;L) = \frac{im_K^2}{E+E_K-m_K}\int d^3\vec{x}e^{-Et_s}j_0(\varphi)I_1^{(L)}(|\vec{x}|^2,t_s), \tag{A7a}$$

$$\tilde{I}_2^{(\ell)}(\rho_1,\rho_2;L) = \frac{im_K^2}{E+E_K-m_K}\int d^3\vec{x}e^{-Et_s}j_0(\varphi)I_2^{(L)}(|\vec{x}|^2,t_s), \tag{A7b}$$

$$\tilde{I}_3^{(\ell)}(\rho_1,\rho_2;L) = \frac{im_K}{E+E_K-m_K}\left[E\int d^3\vec{x}e^{-Et_s}j_0(\varphi)I_2^{(L)}(|\vec{x}|^2,t_s) + |\vec{p}|\int d^3\vec{x}e^{-Et_s}\frac{j_1(\varphi)}{|\vec{x}|}I_3^{(L)}(|\vec{x}|^2,t_s)\right], \tag{A7c}$$

$$\tilde{I}_4^{(\ell)}(\rho_1,\rho_2;L) = \frac{im_K}{E+E_K-m_K}\left[E\int d^3\vec{x}e^{-Et_s}j_0(\varphi)I_2^{(L)}(|\vec{x}|^2,t_s) + |\vec{p}|\int d^3\vec{x}e^{-Et_s}\frac{j_1(\varphi)}{|\vec{x}|}I_4^{(L)}(|\vec{x}|^2,t_s)\right], \tag{A7d}$$

$$\begin{aligned}\tilde{I}_5^{(\ell)}(\rho_1,\rho_2;L) = \frac{im_K}{M(E+E_K-m_K)}\Bigg[&E^2\int d^3\vec{x}e^{-Et_s}j_0(\varphi)I_2^{(L)}(|\vec{x}|^2,t_s)\\ &+|\vec{p}|\int d^3\vec{x}e^{-Et_s}\frac{j_1(\varphi)}{|\vec{x}|}\times\left[EI_3^{(L)}(|\vec{x}|^2,t_s)+EI_4^{(L)}(|\vec{x}|^2,t_s)+I_1^{(L)}(|\vec{x}|^2,t_s)-I_2^{(L)}(|\vec{x}|^2,t_s)\right]\\ &-|\vec{p}|^2\int d^3\vec{x}e^{-Et_s}\frac{j_2(\varphi)}{|\vec{x}|^2}I_5^{(L)}(|\vec{x}|^2,t_s)\Bigg].\end{aligned} \tag{A7e}$$

The scalar functions calculated through the IVR method are given by

$$\tilde{I}_i^{\mathrm{IVR}}(\rho_1,\rho_2;L) = \tilde{I}_i^{(s)}(\rho_1,\rho_2;L) + \tilde{I}_i^{(\ell)}(\rho_1,\rho_2;L), \quad \text{for } i=1,\ldots,5. \tag{A8}$$

As a next step, we perform the finite-volume correction by introducing $\delta_i^{\mathrm{IVR}}(L)$ for each scalar function:

$$\tilde{I}_i(\rho_1,\rho_2) = \tilde{I}_i^{\mathrm{IVR}}(\rho_1,\rho_2;L) + \delta_i^{\mathrm{IVR}}(L). \tag{A9}$$

Here, $\delta_i^{\mathrm{IVR}}(L)$ can be approximated by the kaon- and ρ-state contributions:

$$\delta_i^{\mathrm{IVR}}(L) \approx \tilde{I}_{i,K}^{\mathrm{IVR}}(\rho_1,\rho_2) - \tilde{I}_{i,K}^{\mathrm{IVR}}(\rho_1,\rho_2;L)\tilde{I}_{i,\rho}^{\mathrm{IVR}}(\rho_1,\rho_2) - \tilde{I}_{i,\rho}^{\mathrm{IVR}}(\rho_1,\rho_2;L). \tag{A10}$$

In practice, $\tilde{I}_{i,K}^{\mathrm{IVR}}(\rho_1,\rho_2)$ and $\tilde{I}_{i,\rho}^{\mathrm{IVR}}(\rho_1,\rho_2)$ in the infinite volume can be replaced by $\tilde{I}_{i,K}^{\mathrm{IVR}}(\rho_1,\rho_2;L_\infty)$ and $\tilde{I}_{i,\rho}^{\mathrm{IVR}}(\rho_1,\rho_2;L_\infty)$, with $L_\infty \gg L$.

APPENDIX B: ESTIMATING THE FINITE-VOLUME CORRECTION FROM THE KAON AND ρ STATES

In Eq. (42), the hadronic kernels are defined as

$$\begin{aligned}H_K^{\mu\nu}(\vec{p},t) &= \frac{e^{(E_K-m_K)t}}{2E_K}\langle 0|J_W^\nu(0)|K(p_K)\rangle\langle K(p_K)|J_{\mathrm{em}}^\mu(0)|K\rangle,\\ H_\rho^{\mu\nu}(\vec{p},t) &= \frac{e^{-E_\rho t}}{2E_\rho}\sum_\lambda\langle 0|J_{\mathrm{em}}^\mu(0)|\rho(p_\rho,\lambda)\rangle\langle\rho(p_\rho,\lambda)|J_W^\nu(0)|K\rangle,\end{aligned} \tag{B1}$$

where λ is the polarized direction for the vector meson. $p_K=(iE_K,-\vec{p})$ and $p_\rho=(iE_\rho,\vec{p})$ are the four-momenta for intermediate states with the energies $E_K=\sqrt{\vec{p}^2+m_K^2}, E_\rho=\sqrt{\vec{p}^2+m_\rho^2}$. We define the momentum transfer between the initial kaon and intermediate particles as $q_K=Q-p_K$ and $q_\rho=Q-p_\rho$. The relevant hadronic matrix elements are given by

TABLE V. Momenta used in the determination of the form factors.

$\frac{L}{2\pi}\vec{p}$	(0,0,0)	(0,0,1)	(0,1,1)	(1,1,1)	(0,0,2)
q_K^2 [GeV^2]	0	0.055	0.096	0.131	0.161
q_ρ^2 [GeV^2]	−0.129	0.036	0.178	0.305	0.421

TABLE VI. Determination of the parameters for the form factors.

$\langle r_K^2\rangle$	v	v'	a_1	a_1'	a_2	a'	a''
0.32(2) fm^2	0.58(2)	2.1(2)	0.482(5)	0.30(7)	−0.09(2)	2.2(1)	5.3(4)

$$
\begin{aligned}
\langle 0|J_W^\mu(0)|K(p_K)\rangle &= f_K p_K^\mu,\\
\langle 0|J_{\rm em}^\mu(0)|\rho(p_\rho,\lambda)\rangle &= f_\rho \epsilon^\mu(p_\rho,\lambda),\\
\langle K(p_K)|J_{\rm em}^\mu(0)|K\rangle &= F^{(K)}(q_K^2)(Q+p_K)^\mu,\\
\langle \rho(p_\rho,\lambda)|J_W^\mu(0)|K\rangle &= \frac{2V(q_\rho^2)}{m_K+m_\rho}\varepsilon^{\mu\nu\alpha\beta}\epsilon^\nu(p_\rho,\lambda)p_\rho^\alpha Q^\beta - (m_K+m_\rho)A_1(q_\rho^2)\epsilon^\mu(p_\rho,\lambda)\\
&\quad + \frac{A_2(q_\rho^2)(\epsilon\cdot Q)}{m_K+m_\rho}(Q+p_\rho)^\mu + \frac{2m_\rho A(q_\rho^2)(\epsilon\cdot Q)}{q_\rho^2}(Q-p_\rho)^\mu,
\end{aligned}
\tag{B2}
$$

where f_K and f_ρ are decay constants for K and ρ. $\epsilon^\mu(p_\rho,\lambda)$ is the polarization vector. $F^{(K)}(q^2)$ is the kaon electromagnetic form factor. $V(q^2)$, $A_1(q^2)$, $A_2(q^2)$, and $A(q^2)$ are the form factors for the semileptonic decays, with the convention adopted from Refs. [44,45]. The form factor $A(q^2)$ approaches zero at the limit of $q^2 \to 0$ [44].

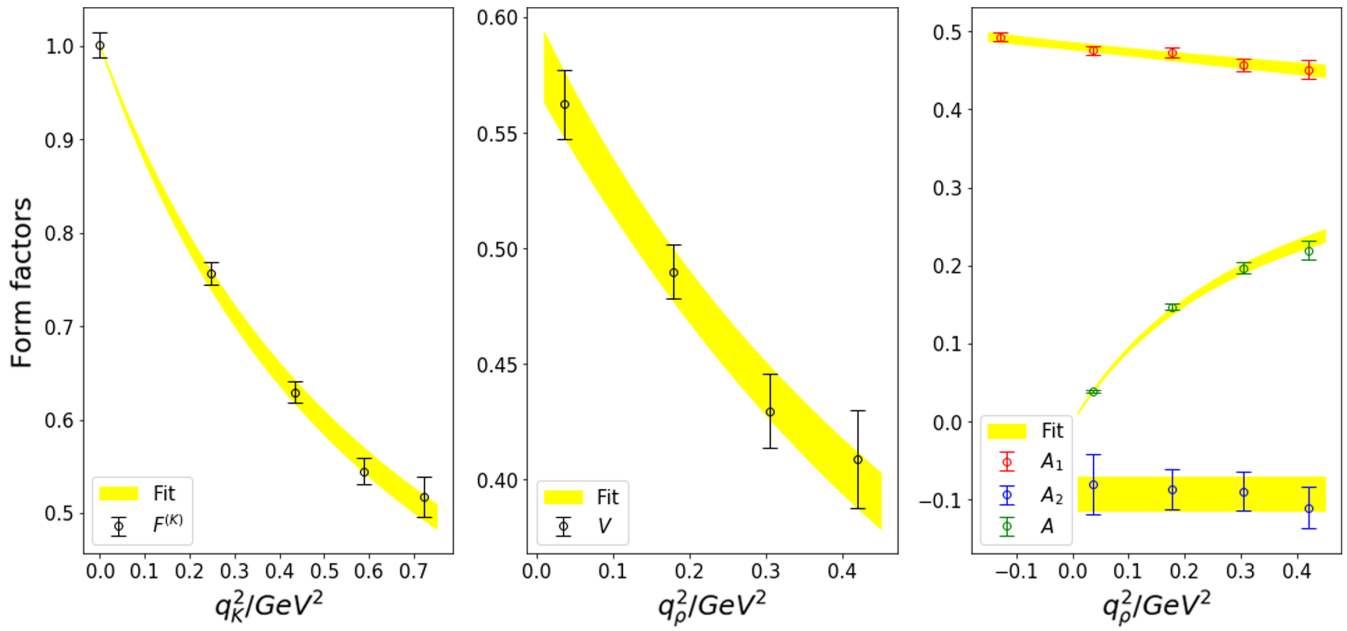

FIG. 13. The lattice results of the form factors together with the fitting curve.

We use the simple parametrization for the above form factors:

$$F^{(K)}(q^2) = \frac{1}{1+\frac{\langle r_K^2\rangle}{6}q^2}, \qquad V(q^2) = \frac{v}{1+v'\frac{q^2}{(m_\rho+m_K)^2}},$$
$$A_1(q^2) = \frac{a_1}{1+a_1'\frac{q^2}{(m_\rho+m_K)^2}}, \quad A_2(q^2) = \frac{a_2}{1+a_2'\frac{q^2}{(m_\rho+m_K)^2}},$$
$$A(q^2) = \frac{a'\frac{q^2}{(m_\rho+m_K)^2}}{1+a''\frac{q^2}{(m_\rho+m_K)^2}}, \tag{B3}$$

with $\langle r_K^2\rangle$ being the square of kaon charge radius and v, v', a_1, a_1', a_2, a_2', a', and a'' as the free parameters.

We calculate the hadronic matrix elements at discrete lattice momenta listed in Table V. Through the fit to the forms [Eq. (B3)], we extract the parameters shown in Table VI. The lattice data together with the fitting curves are plotted in Fig. 13. Once $H^{\mu\nu}_{K/\rho}(\vec{p},t)$ are determined, we can estimate the finite-volume corrections $\delta^{\mathrm{IVR}}_{i,K/\rho}$. Note that the parametrization in Eq. (B3) does bring in the model dependence, but it only affects $\delta^{\mathrm{IVR}}_{i,K/\rho}$. As long as the lattice size is sufficiently large, $\delta^{\mathrm{IVR}}_{i,K/\rho}$ will vanish exponentially.

[1] V. Cirigliano, G. Ecker, H. Neufeld, A. Pich, and J. Portoles, Rev. Mod. Phys. **84**, 399 (2012).
[2] A. J. Buras, Acta Phys. Pol. B **49**, 1043 (2018).
[3] A. A. Poblaguev *et al.*, Phys. Rev. Lett. **89**, 061803 (2002).
[4] H. Ma *et al.*, Phys. Rev. D **73**, 037101 (2006).
[5] J. Bijnens, G. Ecker, and J. Gasser, Nucl. Phys. **B396**, 81 (1993).
[6] C. Geng, I.-L. Ho, and T. Wu, Nucl. Phys. **B684**, 281 (2004).
[7] L. Ametller, J. Bijnens, A. Bramon, and F. Cornet, Phys. Lett. B **303**, 140 (1993).
[8] N. H. Christ, X. Feng, A. Portelli, and C. T. Sachrajda (RBC, UKQCD Collaborations), Phys. Rev. D **93**, 114517 (2016).
[9] Z. Bai, N. H. Christ, X. Feng, A. Lawson, A. Portelli, and C. T. Sachrajda, Phys. Rev. Lett. **118**, 252001 (2017).
[10] Z. Bai, N. H. Christ, X. Feng, A. Lawson, A. Portelli, and C. T. Sachrajda, Phys. Rev. D **98**, 074509 (2018).
[11] N. H. Christ, X. Feng, A. Portelli, and C. T. Sachrajda (RBC, UKQCD Collaborations), Phys. Rev. D **100**, 114506 (2019).
[12] N. H. Christ, X. Feng, L.-C. Jin, and C. T. Sachrajda, Phys. Rev. D **103**, 014507 (2021).
[13] N. H. Christ, X. Feng, A. Portelli, and C. T. Sachrajda (RBC, UKQCD Collaborations), Phys. Rev. D **92**, 094512 (2015).
[14] N. H. Christ, X. Feng, A. Juttner, A. Lawson, A. Portelli, and C. T. Sachrajda, Phys. Rev. D **94**, 114516 (2016).
[15] N. Carrasco, V. Lubicz, G. Martinelli, C. T. Sachrajda, N. Tantalo, C. Tarantino, and M. Testa, Phys. Rev. D **91**, 074506 (2015).
[16] V. Lubicz, G. Martinelli, C. T. Sachrajda, F. Sanfilippo, S. Simula, and N. Tantalo, Phys. Rev. D **95**, 034504 (2017).
[17] D. Giusti, V. Lubicz, G. Martinelli, C. T. Sachrajda, F. Sanfilippo, S. Simula, N. Tantalo, and C. Tarantino, Phys. Rev. Lett. **120**, 072001 (2018).
[18] X. Feng, M. Gorchtein, L.-C. Jin, P.-X. Ma, and C.-Y. Seng, Phys. Rev. Lett. **124**, 192002 (2020).
[19] C.-Y. Seng, X. Feng, M. Gorchtein, and L.-C. Jin, Phys. Rev. D **101**, 111301 (2020).
[20] N. H. Christ, X. Feng, L.-C. Jin, and C. T. Sachrajda, Proc. Sci., LATTICE2019 (**2020**) 259.
[21] A. Desiderio, R. Frezzotti, M. Garofalo, D. Giusti, M. Hansen, V. Lubicz, G. Martinelli, C. T. Sachrajda, F. Sanfilippo, S. Simula, and N. Tantalo, Phys. Rev. D **103**, 014502 (2021).
[22] R. Frezzotti, M. Garofalo, V. Lubicz, G. Martinelli, C. T. Sachrajda, F. Sanfilippo, S. Simula, and N. Tantalo, Phys. Rev. D **103**, 053005 (2021).
[23] C.-Y. Seng, X. Feng, M. Gorchtein, L.-C. Jin, and U.-G. Meißner, J. High Energy Phys. 10 (2020) 179.
[24] P.-X. Ma, X. Feng, M. Gorchtein, L.-C. Jin, and C.-Y. Seng, Phys. Rev. D **103**, 114503 (2021).
[25] N. H. Christ, X. Feng, G. Martinelli, and C. T. Sachrajda, Phys. Rev. D **91**, 114510 (2015).
[26] R. A. Briceño, Z. Davoudi, M. T. Hansen, M. R. Schindler, and A. Baroni, Phys. Rev. D **101**, 014509 (2020).
[27] N. H. Christ, X. Feng, L. Jin, C. Tu, and Y. Zhao, Proc. Sci. LATTICE2019 (**2020**) 128.
[28] X. Feng and L. Jin, Phys. Rev. D **100**, 094509 (2019).
[29] G. Gagliardi, V. Lubicz, G. Martinelli, F. Mazzetti, C. T. Sachrajda, F. Sanfilippo, S. Simula, and N. Tantalo, arXiv: 2202.03833.
[30] K. Kampf, J. Novotný, and P. Sanchez-Puertas, Phys. Rev. D **97**, 056010 (2018).
[31] P. A. Zyla *et al.* (Particle Data Group), Prog. Theor. Exp. Phys. **2020**, 083C01 (2020).
[32] L. Lellouch and M. Luscher, Commun. Math. Phys. **219**, 31 (2001).
[33] H. B. Meyer, Phys. Rev. Lett. **107**, 072002 (2011).
[34] X. Feng, S. Aoki, S. Hashimoto, and T. Kaneko, Phys. Rev. D **91**, 054504 (2015).
[35] C. Andersen, J. Bulava, B. Hörz, and C. Morningstar, Nucl. Phys. **B939**, 145 (2019).
[36] F. Erben, J. R. Green, D. Mohler, and H. Wittig, Phys. Rev. D **101**, 054504 (2020).
[37] X. Feng, L. Jin, and M. J. Riberdy, Phys. Rev. Lett. **128**, 052003 (2022).
[38] X.-Y. Tuo, X. Feng, and L.-C. Jin, Phys. Rev. D **100**, 094511 (2019).

[39] X. Feng, Y. Fu, and L.-C. Jin, Phys. Rev. D **101**, 051502 (2020).
[40] Y. Meng, X. Feng, C. Liu, T. Wang, and Z. Zou, arXiv: 2109.09381.
[41] Y. Fu, X. Feng, L.-C. Jin, and C.-F. Lu, arXiv:2202.01472.
[42] M. Tanabashi *et al.* (Particle Data Group), Phys. Rev. D **98**, 030001 (2018).
[43] C. Alexandrou *et al.*, Phys. Rev. D **98**, 054518 (2018).
[44] J. D. Richman and P. R. Burchat, Rev. Mod. Phys. **67**, 893 (1995).
[45] K. C. Bowler, J. F. Gill, C. M. Maynard, and J. M. Flynn (UKQCD Collaboration), J. High Energy Phys. 05 (2004) 035.